

RESEARCH ARTICLE

Human iPSC-derived astrocytes generated from donors with globoid cell leukodystrophy display phenotypes associated with disease

Richard Lieberman^{1*}, Leslie K. Cortes^{1*}, Grace Gao¹, Hyejung Park², Bing Wang², Patrick L. Jones¹, R. Bridge Hunter¹, John P. Leonard¹, Robert H. Barker, Jr.¹

1 Lysosomal Storage and Metabolic Disease Cluster, Rare and Neurologic Disease Therapeutic Area, Sanofi, Framingham, MA, United States of America, **2** US Early Development, Sanofi, Waltham, MA, United States of America

* Lieberman.rich@gmail.com (RL); Lesliekcortes@gmail.com (LKC)



OPEN ACCESS

Citation: Lieberman R, Cortes LK, Gao G, Park H, Wang B, Jones PL, et al. (2022) Human iPSC-derived astrocytes generated from donors with globoid cell leukodystrophy display phenotypes associated with disease. *PLoS ONE* 17(8): e0271360. <https://doi.org/10.1371/journal.pone.0271360>

Editor: Srinivas Mummidi, The University of Texas Rio Grande Valley, UNITED STATES

Received: February 20, 2022

Accepted: June 28, 2022

Published: August 3, 2022

Copyright: © 2022 Lieberman et al. This is an open access article distributed under the terms of the [Creative Commons Attribution License](https://creativecommons.org/licenses/by/4.0/), which permits unrestricted use, distribution, and reproduction in any medium, provided the original author and source are credited.

Data Availability Statement: All relevant data are within the paper and its [Supporting Information](#) files.

Funding: The authors received no specific funding for this work.

Competing interests: I have read the journal's policy and the authors of this manuscript have the following competing interests: At the time the research was conducted, all authors were employed by Sanofi. GG, HP, and BW are currently

Abstract

Globoid cell leukodystrophy (Krabbe disease) is a fatal neurodegenerative, demyelinating disease caused by dysfunctional activity of galactosylceramidase (GALC), leading to the accumulation of glycosphingolipids including psychosine. While oligodendrocytes have been extensively studied due to their high levels of GALC, the contribution of astrocytes to disease pathogenesis remains to be fully elucidated. In the current study, we generated induced pluripotent stem cells (iPSCs) from two donors with infantile onset Krabbe disease and differentiated them into cultures of astrocytes. Krabbe astrocytes recapitulated many key findings observed in humans and rodent models of the disease, including the accumulation of psychosine and elevated expression of the pro-inflammatory cytokine IL-6. Unexpectedly, Krabbe astrocytes had higher levels of glucosylceramide and ceramide, and displayed compensatory changes in genes encoding glycosphingolipid biosynthetic enzymes, suggesting a shunting away from the galactosylceramide and psychosine pathway. In co-culture, Krabbe astrocytes negatively impacted the survival of iPSC-derived human neurons while enhancing survival of iPSC-derived human microglia. Substrate reduction approaches targeting either glucosylceramide synthase or serine palmitoyltransferase to reduce the sphingolipids elevated in Krabbe astrocytes failed to rescue their detrimental impact on neuron survival. Our results suggest that astrocytes may contribute to the progression of Krabbe disease and warrant further exploration into their role as therapeutic targets.

Introduction

Krabbe disease (globoid cell leukodystrophy) is a rare lysosomal storage disorder characterized by severe demyelination, neurodegeneration, and progressive motor and cognitive deterioration that results from dysfunctional activity of galactosylceramidase (GALC) [1, 2]. Histologically, the brains of Krabbe disease patients are noted for the appearance of multinucleated globoid cells, loss of myelin, and prominent gliosis within the white matter [3]. Deficiency of

employed by Sanofi. This does not alter our adherence to PLOS ONE policies on sharing data and materials.

GALC arises due to mutations in its gene, *GALC* [4–6], leading to impaired degradation of the glycosphingolipid galactosylceramide [7, 8]. Accumulation of galactosylceramide does not directly result in neuropathology, but rather it is its byproduct psychosine (galactosylsphingosine), generated via the lysosomal actions of acid ceramidase, that is thought to be the pathogenic driver of disease [7, 9, 10]. Indeed, higher concentrations of psychosine are observed in the severe early onset form of the disease compared to the less severe late onset forms, and reduced psychosine levels correlate with the therapeutic benefit of allogenic hematopoietic stem cell transplantation [11, 12].

Cytotoxicity of psychosine is mediated through multiple, broad mechanisms. This includes disruption of lysosomal pH [13], perturbation of cellular membrane and lipid raft architecture [14, 15], inhibition of protein kinase C activity [16], generation of toxic lysophosphatidylcholine (LPC) via the actions of phospholipase A2 [17, 18], depolarization of mitochondrial membrane potential [19], and induction of inflammatory cytokines and upregulation of nitric oxide synthase (iNOS) [20, 21]. In the central nervous system, oligodendrocytes are particularly sensitive to impairments of GALC enzyme activity and psychosine exposure, as galactosylceramide is highly expressed in myelinating cells [5, 22]. Since Krabbe disease is hallmarked by robust white matter pathology including demyelination and a near complete loss of oligodendrocytes [23], these cells have been the primary focus of research examining the effects of psychosine on cellular perturbations related to disease progression. However, other neural cell types are sensitive to *GALC* mutations and are negatively affected by elevated psychosine in the disease state, including neurons [24–27], microglia [28–31], and astrocytes [18, 31–34]. Together these results suggest that numerous cell types may be implicated disease pathology, which warrants further investigation into how complex interactions between cells of the brain might be perturbed in Krabbe disease.

In the context of Krabbe disease, *GALC* deficient murine oligodendrocytes derived from the *twitcher* mouse [35] were able to survive and myelinate axons when implanted into the myelin-deficient *shiverer* mouse [36], suggesting, in part, that non-cell autonomous factors can influence Krabbe oligodendrocyte survival. Indeed, the effects of astrocytes have been implicated in disease pathogenesis through two seminal findings; First, the astrocytic extracellular protease MMP-3 (matrix metalloproteinase-3) is significantly upregulated in the *twitcher* mouse and its expression influences microglia to form the namesake globoid cells observed in Krabbe disease [28]. Second, the enzyme that synthesizes the neuroinflammatory mediator prostaglandin D2 (HPDGS) is increased in *twitcher* microglia, and its receptor, prostaglandin DP1, is upregulated in activated *twitcher* astrocytes. HPDGS inhibition or genetic ablation of the DP1 receptor ameliorated disease phenotypes including astrogliosis, demyelination, and oligodendrocyte apoptosis in the rodent model [37]. Overall, the contribution of astrocytes to the pathology of leukodystrophies is of expanding interest [38], sparked by findings that mutations specifically in astrocyte-expressing glial-fibrillary acidic protein (GFAP) gene cause demyelinating Alexander disease [39], defective support and differentiation of astrocytes results in vanishing white matter disease [40–42], and astrocyte dysfunction precedes demyelination observed in X-linked adrenoleukodystrophy [43], among many others [44, 45]. Therefore, examination of how Krabbe astrocytes impact neurons and microglia warrant further study, particularly in the setting of human Krabbe patient-derived cells.

iPSCs generated from human fibroblasts [46] offer the ability to differentiate patient-derived, disease-relevant cell types. While the murine model of Krabbe disease recapitulates aspects of the human condition [35], and iPSCs have been generated from these mice for differentiation into disease-specific cell types *in vitro* [47], generation of human-derived cell types relevant to Krabbe disease may provide valuable insight into novel mechanisms related to disease progression. For example, a recent study demonstrated *GALC*-dependent

psychosine accumulation and defective differentiation of human iPSCs into a mixed population of neurons, astrocytes, and oligodendrocyte precursors [48]. Additional studies are needed to elucidate cellular mechanisms implicated in neuropathology, including experiments designed to examine effects of GALC mutations of specific cell types, including astrocytes.

To this end, the goal of the current study was to explore Krabbe-associated phenotypes in human iPSC-derived astrocytes. The ability of iPSC-derived astrocytes to recapitulate key findings observed in Krabbe human and mouse studies was validated. Perturbations in lipid levels and lipid biosynthesis genes were observed. Methods to co-culture astrocytes and neurons and astrocytes and microglia of different genetic backgrounds were established and used to identify disease-relevant phenotypes. Finally, this culture system allowed us to explore the utility of substrate reduction approaches that aim to normalize perturbed lipid levels. Overall, the results of our study add to the existing understanding of Krabbe disease and further implicate astrocytes as a contributing cell type to Krabbe disease progression.

Materials and methods

Generation of iPSCs

Cells derived from three healthy controls and two donors with infantile onset Krabbe disease were obtained from commercial vendors for reprogramming into iPSCs. Details for the cell lines are as follows: Control 1 (Coriell, GM05659, 1 year old male, Caucasian), Control 2 (Lonza, CC-2511, 31 year female, Caucasian), Control 3 (Icelltis, HUCMF05, male cord blood), Krabbe 1 (Coriell, GM06806, 2 year female, Caucasian), and Krabbe 2 (Coriell, GM01773, 1 year male, Caucasian). Both Krabbe fibroblasts lines were homozygous for a ~30 kb deletion in *GALC* resulting in the loss of exons 11–17, which is the most common mutation associated with Krabbe disease in Caucasians and results in a severe infantile onset form of the disease [49]. Quantitative polymerase chain reaction (qPCR) using TaqMan probe and primer sets designed for specific intron/exon boundaries confirmed the genetic characterization of the cell lines. No detectable expression of *GALC* mRNA was observed between exons 13–16 in the Krabbe fibroblasts (S1 Fig).

Reprogramming to pluripotency was performed using the CytoTune 2.0 sendai virus kit (Thermo-Fisher Scientific) to overexpress four transcription factors (OCT4, SOX2, KLF4, and c-Myc) following the manufacturer's protocol. Individual colonies that formed following viral transduction were manually selected and expanded as clones on Matrigel (Corning) coated plates using mTeSR1 culture medium (StemCell Technologies). One clone was used per donor subject. Expression of pluripotency markers OCT4 and NANOG were validated using immunocytochemistry. G-banded karyotyping was performed by the WiCell Institute (Madison, WI). All iPSC lines used in the current study displayed a normal karyotype.

Differentiation of neurons and astrocytes

Neural progenitor cells (NPCs) were differentiated from healthy control and Krabbe iPSCs using a dual-SMAD inhibition approach [50, 51]. When iPSCs grown on Matrigel coated plates reached ~20–30% confluence, medium was switched to neural induction medium 1 containing a 50/50 mixture of Advanced DMEM/F12 (Thermo-Fisher Scientific) and Neurobasal (Thermo-Fisher Scientific) supplemented with 1x N2 Supplement (Thermo-Fisher Scientific), 1X B27 Supplement (Thermo-Fisher Scientific), 1X GlutaMAX (Thermo-Fisher Scientific), 10 ng/mL human leukemia inhibitory factor (Millipore), 3 μ M CHIR99021 (Stemgent), 2 μ M SB432542 (Stemgent), 2 μ M Dorsomorphin (StemCell Technologies), and 0.1 μ M Compound E (StemCell Technologies). Medium was fully replaced daily for 2 days, following which cells were switched to neural induction medium 2, which was the same as described

above without the addition of 2 μ M Dorsomorphin, for an additional 5 days, with medium replaced daily. NPCs were dissociated using Accumax (Millipore), counted, and 2.5 million cells were seeded onto Matrigel (Corning) coated 10 cm dishes in neural induction maintenance medium (as describe above without the additions of 0.1 μ M Compound E and 2 μ M Dorsomorphin). Maintenance medium was replaced daily, and NPCs were passaged onto fresh Matrigel coated dishes using Accumax every 5–7 days when they reached confluency. After 2–3 passages, NPCs were cryopreserved in mFreSR (StemCell Technologies) for subsequent differentiation into neuron and astrocyte cultures. Successful differentiation of NPCs was validated using immunocytochemistry for Nestin and SOX2.

Neuronal differentiation was performed using an established protocol that generates electrophysiologically-active neurons enriched for tyrosine hydroxylase positive dopamine neuron subtypes [51]. NPCs from the healthy controls and Krabbe donors were seeded onto Matrigel coated 10 cm dishes at a density of 800,000 cells per plate in neural induction maintenance medium supplemented with 5 μ M Y-27632 (StemCell Technologies). The following day, medium was aspirated and replaced with neural differentiation medium 1 consisting of DMEM/F12 supplemented with 1X N2 Supplement, 1X B27 Supplement, 1X penicillin-streptomycin, 300 ng/mL cAMP (Sigma-Aldrich), 2 mM vitamin C (Sigma-Aldrich), 100 ng/mL sonic hedgehog (SHH, R&D Systems), and 100 ng/mL FGF-8b (Peprotech). Medium was fully replaced every other day for 11 days. On Day 11, medium was aspirated and replaced with neural differentiation medium 2, consisting of DMEM/F12 supplemented with 1X N2 Supplement, 1X B27 Supplement, 1X penicillin-streptomycin, 300 ng/mL cAMP, 2mM vitamin C, 500 μ M dibutyryl cAMP (Sigma-Aldrich), 10 ng/mL of each brain-derived neurotrophic factor (BDNF, R&D Systems), glial-derived neurotrophic factor (GDNF, R&D Systems), and insulin-like growth factor-1 (IGF-1, Peprotech), 1 ng/mL TGF- β 3 (R&D Systems), and 1 μ g/mL laminin (Sigma-Aldrich). Medium was replaced every other day for 5 days. On Day 16 (D16) neuronal cultures were dissociated using Accumax and cryopreserved in complete neural differentiation medium 2 supplemented with 10% DMSO. Characterization of neural cultures by immunocytochemistry on Day 23 revealed expression of pan-neuronal markers HuC/D, Tuj1, and MAP2 (S2A Fig). Quantification revealed ~ 80% HuC/D+ terminally differentiated neurons and ~ 20% SOX2+ NPCs (S2B Fig). No robust difference was observed in the morphology of control and Krabbe TUJ1+ and MAP2+ neurons. Consistent with the published protocol [51], our neuronal cultures contained a subset of tyrosine hydroxylase positive dopamine neurons, highlighted in orange in the middle row of S2A Fig.

Astrocytes were differentiated following previously described methods [52] that utilize the “spontaneous emergence approach” [53], whereby extended culture of mixed neurons and NPCs leads to the emergence of astrocytes that can be expanded. Day 16 cryopreserved neuron/NPCs were thawed onto poly-L-ornithine (10 μ g/mL, Sigma-Aldrich) and laminin (10 μ g/mL, Sigma-Aldrich) coated 10 cm dishes at a density of ~ 2.5 million cells per plate in NDM-2 medium supplemented with 5 μ M Y-27632. The following day medium was replaced with NDM-2 without the addition of Y-27632. 50% medium changes were performed every 3 days for an additional 21 days to allow for the spontaneous generation of astrocytes. On Day 38 of differentiation, cells were dissociated using Accumax and plated 1:2 onto poly-L-ornithine and laminin coated 10 cm dishes in astrocyte differentiation medium consisting of Advanced DMEM/F12 supplemented with 1X B27 Supplement, 1X penicillin-streptomycin, 1X GlutaMAX, 1% FBS (Thermo-Fisher Scientific), and 2 μ g/mL Heparin (Sigma-Aldrich). Astrocyte differentiation medium (ADM) was fully replaced three times per week. Astrocytes were expanded in ADM until confluency (~7 days) and passaged 1:3 until Day 63–65 (D63–65), following which astrocyte cultures were dissociated with Accumax and cryopreserved in ADM supplemented with 10% DMSO.

Differentiation of microglia

Microglia-like cells were differentiated from Control 1 and Control 3 donors as described [54–56]. Embryoid bodies (EBs) were generated from confluent iPSC cultures by dissociating them to single cells and seeding at a density of $\sim 4 \times 10^6$ cells per well of Aggrewell 800 6-well plates (StemCell Technologies) in EB medium consisting of complete mTeSR1 supplemented with 10 μ M Y27632 (StemCell Technologies), 50 ng/mL BMP-4, 20 ng/mL stem cell factor (SCF), and 50 ng/mL VEGF-121 (all from Peprotech). EB medium was replaced every other day for 7 days. EBs were collected from the Aggrewell plates, passed through a 40 μ m filter, centrifuged, and resuspended in hematopoietic cell medium consisting of X-VIVO 15 medium (with gentamicin and phenol red) supplemented with 2 mM Glutamax, 1X penicillin/streptomycin, 55 μ M β -mercaptoethanol (Gibco), 100 ng/mL M-CSF (Peprotech), and 25 ng/mL IL-3 (Cell Guidance Systems). EBs were seeded into tissue culture treated flask at a density of 150 EBs per T150 flask. An equal volume of fresh hematopoietic cell medium was added to the cultures on Days 7 and 14 following seeding, with no medium being removed. Thereafter, $\sim 75\%$ of the medium was collected and replaced with fresh hematopoietic cell medium every 7 days. Primitive macrophage precursors (PMPs) were harvested during the medium change by collecting supernatant and passing it through a 40 μ m filter. Cells were centrifuged and resuspended in microglia medium consisting of Advanced DMEM/F12 supplemented with 2mM Glutamax, 1X penicillin/streptomycin, 1X N2 supplement, 100 ng/mL IL-34, and 10ng/mL GM-CSF (both from Peprotech). PMPs were seeded into tissue culture treated 15 CM plates at 7.5 million cells/plate for terminal differentiation and fresh microglia medium was fully replaced every 2–3 days for 7 days, following which microglia were removed from the plate by incubating with Accumax and a lifting with a cell scraper. Microglia were collected, centrifuged, and frozen in complete microglia medium supplemented with 10% DMSO. Successful differentiation was confirmed using antibodies against IBA1 and CD11b.

Establishment of co-culture models and compound treatment

Cryopreserved astrocytes were seeded onto poly-L-ornithine (10 μ g/mL, Sigma-Aldrich) and laminin (10 μ g/mL, Sigma-Aldrich) CellCarrier Ultra high content imaging plates (PerkinElmer) in complete astrocyte differentiation medium at 10,000 cells/well in 96-well format. Cells were cultured to confluency for 3–7 days prior to establishment of co-culture. Astrocyte medium was aspirated and cryopreserved neurons generated from the Control 1 or Control 2 donor were seeded in NDM-2 at a density of 60,000 cells/well. Cryopreserved microglia generated from the Control 1 or Control 3 donor were seeded in complete microglia medium at a seeding density of 60,000 cells/well. Co-cultures were maintained for 96 hours prior to medium aspiration and fixation in 4% paraformaldehyde for immunocytochemistry analysis described below.

To examine the effects of glucosylceramide synthase (GCS) and serine palmitoyltransferase (SPTLC1) inhibition on neuron cell count in the co-culture paradigm, cryopreserved astrocytes were first seeded onto poly-L-ornithine (10 μ g/mL, Sigma-Aldrich) and laminin (10 μ g/mL, Sigma-Aldrich) 96-well CellCarrier Ultra high content imaging plates (PerkinElmer) in complete astrocyte differentiation medium. The following day, medium was fully replaced with astrocyte differentiation medium containing the indicated concentration of compounds. The GCS inhibitor in the current study was an internal compound and used at its IC₉₉ of 18nM. The SPTCL1 inhibitor Myriocin was purchased from Sigma-Aldrich and used at a range of concentrations (100 nM, 1 μ M and 10 μ M). Compounds were applied to astrocyte mono-cultures for 3–6 days prior to establishment of neuron co-culture, with 50% of medium replaced after 3 days. For co-cultures, astrocyte medium was aspirated and replaced with

complete NDM-2 medium containing 2X each compound. 60,000 control donor-derived neurons were then seeded directly in an equal volume of NDM-2 to dilute compounds to working concentrations. Co-cultures were maintained for 3–4 days prior to assay via immunocytochemistry.

Astrocyte conditioned media effect on neuron viability

Cryopreserved astrocytes from Control and Krabbe donors were seeded onto poly-L-ornithine (10 µg/mL, Sigma-Aldrich) and laminin (10 µg/mL, Sigma-Aldrich) 96 well CellCarrier Ultra high content imaging plates (PerkinElmer) in complete astrocyte differentiation medium at 10,000 cells/well. Following 3 weeks of culture, with 50% astrocyte medium replaced twice per week, medium was fully replaced with complete NDM-2 and conditioned for 96 hours. At this time, cryopreserved neurons from the Control 2 donor were seeded at 10,000 cells/well onto a poly-L-ornithine (10 µg/mL, Sigma-Aldrich) and laminin (10 µg/mL, Sigma-Aldrich) 384-well CellCarrier Ultra high content imaging plate (PerkinElmer) in NDM-2. Following 96-hours of culture, astrocyte conditioned medium was collected and medium from the neurons was aspirated and replaced with the astrocyte conditioned medium. After 96-hours of exposure to astrocyte conditioned medium, neuron viability was quantified by incubating with Calcein Green AM, NucRed Dead, and Hoechst fluorescent probes in PBS +magnesium +calcium for 10 minutes at 37C and imaging on a PerkinElmer Opera Phenix microscope. Cells were imaged with a 20X objective and viability was calculated as the percentage of Calcein Green AM positive, NucRed Dead negative nuclei over the total nuclei (identified with Hoechst) using associated Perkin Elmer Harmony software.

Stimulation of astrocytes with TNF α

Astrocytes from two control and two Krabbe donors were thawed and seeded into a poly-L-ornithine (10 µg/mL, Sigma-Aldrich) and laminin (10 µg/mL, Sigma-Aldrich) coated 96 well plate in complete astrocyte medium and cultured for 7 days, with 50% medium changed after 3 days. Astrocyte cultures were treated with 50 ng/mL TNF α (Sigma-Aldrich) diluted in complete astrocyte medium, or mock medium as a control. Cells were incubated with TNF α for 24 hours, following which medium was aspirated and cells were harvested for RNA expression via qPCR using the Fast Cells-to-Ct kit (Thermo-Fisher Scientific) as described below.

Immunocytochemistry

Mono-cultures and co-cultures of cells from Control and Krabbe donors were fixed in 4% paraformaldehyde for 15 minutes at room temperature, washed twice with PBS, and blocked and permeabilized in 10% normal goat serum (Thermo-Fisher Scientific) (or donkey serum (Sigma-Aldrich) if a goat-derived primary antibody was used) supplemented with 0.3% triton X-100 (Sigma-Aldrich) for 15 minutes at room temperature. Following aspiration of blocking solution, primary antibodies were added in antibody dilution buffer consisting of 2% normal goat serum (or donkey serum (Sigma-Aldrich) if a goat-derived primary antibody was used), 1% bovine serum albumin (Sigma-Aldrich) and 0.1% TWEEN-20 (Sigma-Aldrich) in PBS. The following primary antibodies were used: goat anti-IBA1 (1:500, Abcam Ab5076), mouse anti-HuC/D (1:100, Thermo-Fisher Scientific A21271), rabbit anti-MAP2 (1:500 Ab32454), mouse anti-Tuj1 (1:2000, Millipore MAB1637), rabbit anti-SOX2 (1:500, Millipore, Ab5603), mouse anti-CD44 (1:500, BD Biosciences 550392), rabbit anti-S100 β (1:100, Abcam Ab52642), mouse anti-vimentin (1:1000, Sigma-Aldrich V2258), and mouse anti-GLAST (1:100, Abcam Ab416). Primary antibodies were incubated overnight at 4°C, following which cells were washed four times in PBS and donkey anti-rabbit 488, donkey anti-mouse 568, or donkey

anti-goat 568 Alexa Fluor-conjugated secondary antibodies (diluted 1:1,000 in antibody dilution buffer; Thermo-Fisher Scientific) were applied at room temperature for 2 hours. Cells were washed four times with PBS and counterstained with Hoechst 33342 (1:10,000; Thermo-Fisher Scientific) and CellMask Deep Red (1:10,000; Thermo-Fisher Scientific) diluted in PBS for 10 minutes at room temperature, following which cells were washed two times with PBS and imaged on a Perkin Elmer Opera Phenix microscope. Quantification of cells in co-culture was performed on the associated Perkin Elmer Harmony software to examine the total number of Hoechst positive nuclei that co-stained with either HuC/D (for neurons) or IBA1 (for microglia) per field of view. Images were acquired with a 20X objective, and 9 fields of view were imaged in 3–6 replicate wells per condition, per donor subject, for quantification.

Analysis of sphingolipids

Quantitative analysis of sphingolipids was performed by using liquid chromatography with tandem mass spectrometry analysis (LC-MS/MS). To extract ceramide, glucosylceramide, galactosylceramide, and psychosine, an extraction solution containing 0.2% Formic Acid; 5mM Ammonium formate in (50:50) Methanol:Acetonitrile (v/v) with internal standards was used. D35 labeled C18 galactosylceramide (Matreya), C12 ceramide, and D5 labeled psychosine (Avanti Polar Lipids) were used for internal standards. Ceramide, glucosylceramide, OH-glucosylceramide, galactosylceramide, and OH-galactosylceramide were separated using a Thermo Fisher Scientific LX-2 Multiplex system (ThermoFisher Scientific) and Waters Cortecs HILIC column (2.1 mm x 100 mm, 2.7 μ m particles, Waters Corp.) and analyzed by an API 5000 triple quadrupole mass spectrometer in MRM mode (Applied Biosystems). Psychosine were separated using a waters Acquity UPLC system and BEH HILIC column (2.1 mm x 100 mm, 1.7 μ m particles, Waters Corp.) and analyzed by an API 6500 triple quadrupole mass spectrometer in MRM mode (Applied Biosystems). Calibration curves were generated with C16 ceramide, C16 glucosylceramide, C16 galactosylceramide, and psychosine standards (Avanti Polar Lipids, Alabaster, AL).

To examine basal levels of lipids, D16 neurons and D63–65 astrocytes from 2 healthy controls and 2 Krabbe donors were seeded from cryopreservation onto poly-L-ornithine (10 μ g/mL, Sigma-Aldrich) and laminin (10 μ g/mL, Sigma-Aldrich) coated 24 well plates at a density of 400,000 cells per well for neurons and 200,000 cells/well for astrocytes. To allow comparison between cell types and to control for potential medium effects all cells were seeded and cultured in complete NDM-2 described above. Cells were maintained in culture for 7 days, then were lifted from the plate with Accumax (Millipore), counted, and pelleted via centrifugation. Cell pellets were stored at -80°C until lipid extraction. Extraction was performed proportional to cell number at a ratio of 10 μ L extraction solution / 10,000 cells to normalize to cell number. Extraction solution (described above) was added to cell pellets, vortexed for 3 minutes at 1500 RPM, centrifuged for 5 minutes at 1000 RPM, and then transferred to a 384 well plate for analysis.

To examine lipid levels following compound treatments described above, on the day of takedown medium was aspirated from astrocytes cultured in 96 well plates and replaced with PBS containing Hoechst 33342 (1:1000, Thermo-Fisher Scientific) and Calcein Green AM (50 μ g vial resuspended in 50 μ L DMSO, 1:1000, Thermo-Fisher Scientific) for 10 minutes at 37°C. Cells were washed 3X with PBS and the entire well imaged using a 5X objective on a Perkin Elmer Opera Phenix high content microscope. The number of Calcein Green AM positive viable nuclei was quantified using Perkin Elmer Harmony software. After imaging, PBS was aspirated and cells were dried in a cell culture hood for ~ 2 hours prior to storage in -80°C until lipid extraction. Lipids were extracted by adding 150 μ L extraction buffer (described

above) per well, incubating for 5 minutes at room temperature, spinning down the plate and then transferring the extract to a 384 well plate for analysis.

Gene expression analysis via qPCR

RNA was harvested from astrocytes cultured in 96 well plates using a Fast Cells-to-Ct kit (Thermo-Fisher Scientific, #4399003), per the manufacturer's instructions. Briefly, medium was aspirated and cells were lysed with 50 μ L lysis buffer supplemented with DNase for 10 minutes with agitation, followed by incubation with 5 μ L stop solution for two minutes, with agitation. Lysate was stored at -80° until use. 50 μ L of cDNA was synthesized using 10 μ L input cell lysate mixed with reverse transcription buffer and enzyme mix, per the kit instructions. Reverse transcription cycles were as follows: 37°C for 60 minutes followed by 95°C for 5 minutes. Two μ L of cDNA was used as input into a 10 μ L real time PCR reaction consisting of 0.5 μ L each FAM- and VIC-labeled TaqMan probe and primer sets, 5 μ L Fast Advanced real time Master Mix (Thermo-Fisher Scientific), and 2 μ L nuclease free water. Real time PCR was performed on an Applied Biosystems QuantStudio 7 instrument with the following cycles: 95°C for 20 sec, followed by 40 cycles of 95°C for 3 sec and 60°C for 30 sec. The following TaqMan probes were used in our study (all from Thermo-Fisher Scientific): FAM-labeled *IL6* (Hs00174131_m1), *IL8* (*CXCL8*, Hs00174103_m1), *IL1B* (Hs01555410_m1), *CCL2* (*MCP-1*, Hs00234140_m1), *ASAH1* (Hs00602774_m1), *UGT8* (Hs00409958_m1), *UGCG* (Hs00916612_m1), *GBA* (*GBA1*, Hs00986836_g1), *RIPK3* (Hs00179132_m1), and *MTIE* (Hs01652848_g1). Gene expression for targets of interest were normalized to VIC-labeled 18s rRNA (Thermo-Fisher Scientific, 4319413E). Relative expression was calculated on the QuantStudio software using the ddCt method with the value 1 being set to the Control 1 donor.

IL-6 protein analysis via AlphaLISA

IL-6 protein was measured in the supernatant of astrocyte-conditioned medium. Undiluted supernatant was collected following the indicated culture times and analyzed on a PHERAstar plate reader (BMG Labtech) using an AlphaLISA IL-6 kit (Perkin Elmer), per the manufacturer's instructions. Concentration of IL-6 was calculated based on the standard curve provided in the AlphaLISA kit. Following collection of the supernatant, cells were live imaged with Calcein Green AM and Hoechst to quantify cell number. PBS containing calcium and magnesium supplemented with Hoechst 33342 (1:1000, Thermo-Fisher Scientific) and Calcein Green AM (50 μ g vial resuspended in 50 μ L DMSO, 1:1000, Thermo-Fisher Scientific) was applied to the cultures for 10 minutes at 37°C . Cells were washed 3X with PBS and the entire well was imaged using a 5X objective on a Perkin Elmer Opera Phenix high content microscope. The number of Calcein Green AM positive nuclei were quantified using Harmony software and used to normalize protein expression values to determine IL-6 concentration on a per-viable cell basis.

Statistical analysis

Statistical analysis was performed using GraphPad Prism (GraphPad Prism version 8.3.1 for Windows, GraphPad Software, San Diego, California USA, www.graphpad.com). Unpaired Student's t-tests were used to compare basal glycosphingolipids, gene expression, and number of cells in co-culture between Control and Krabbe cells. Statistics were performed on grouped data (i.e. Control vs. Krabbe), but the data is visualized per subject for the reader to observe between-line differences. Gene expression following TNF α stimulation was assessed using two-way ANOVA on pooled values comparing Control and Krabbe donors. Treatment (TNF α) and Genotype (Control vs. Krabbe) were set as the factors for the two-way ANOVA. A Bonferroni's multiple comparison post-hoc test was performed specifically comparing

Control and Krabbe gene expression values following TNF α stimulation. The effects of compound treatment on lipid levels, IL-6 protein expression, and the number of HuC/D+ nuclei was analyzed by two-way ANOVA with a Bonferroni multiple comparison post-hoc test comparing DMSO and treatment conditions within a given cell line. For all tests, statistical significance was determined as $p < 0.05$, or adjusted $p < 0.05$ for the Bonferroni multiple comparison's tests.

Results

Krabbe iPSC-derived astrocytes recapitulate findings from rodent and human models of disease

iPSCs from three healthy controls and two donors with infantile onset Krabbe disease successfully differentiated into astrocytes that expressed appropriate lineage markers vimentin, S100 β , CD44, and GLAST (Fig 1). No apparent difference in expression patterns were noted between cell lines, and following seeding onto laminin coated plates astrocytes from all donors proliferated and formed confluent monolayers. We validated the utility of our human iPSC model by asking if they recapitulated some established findings in the field. Compared to controls, Krabbe astrocytes had higher expression of *RIPK3* and *MT1E* transcripts ($t = 5.8$, $p < 0.0001$, and $t = 7.9$, $p < 0.0001$, respectively) (S3 Fig), as previously reported in rodent and human models [57, 58]. While undetectable in the control astrocytes, mRNA and protein expression of IL-6 was detected in unstimulated Krabbe astrocytes (mRNA: $t = 7.0$, $p < 0.0001$; Protein: $t = 7.3$, $p < 0.0001$) (Fig 2). mRNA expression of *IL-6*, *IL-8*, *IL-1 β* , and *MCP-1 (CCL2)* was profiled following 24-hour TNF α stimulation in control and Krabbe astrocyte cultures. Two-way ANOVA revealed an overall significant effect of TNF α treatment (all $p < 0.0001$), an overall significant effect of donor genotype (all $p < 0.0001$, except for *IL-1 β* , $p < 0.001$), and a significant interaction between treatment and genotype (all $p < 0.0001$, except for *IL-1 β* , $p < 0.001$) for all four gene examined (S4A–S4D Fig), suggesting that Krabbe astrocytes responded differently to TNF α than control astrocytes. Post-hoc analysis identified that Krabbe astrocytes had

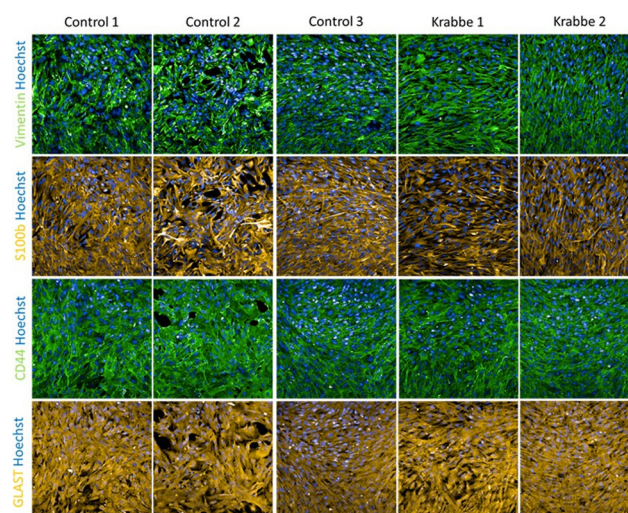


Fig 1. Assessment of differentiation into astrocyte lineage. Representative images of astrocytes differentiated from 3 healthy control donors and 2 donors with infantile onset Krabbe disease caused by a large deletion in the *GALC* gene. Cryopreserved astrocytes were thawed and cultured for 7 days prior to fixation and imaging. Immunocytochemistry revealed positive staining for astrocyte markers vimentin, s100 β , CD44, and GLAST (EAAT1) in all cell lines used. Images were taken at 20x magnification.

<https://doi.org/10.1371/journal.pone.0271360.g001>

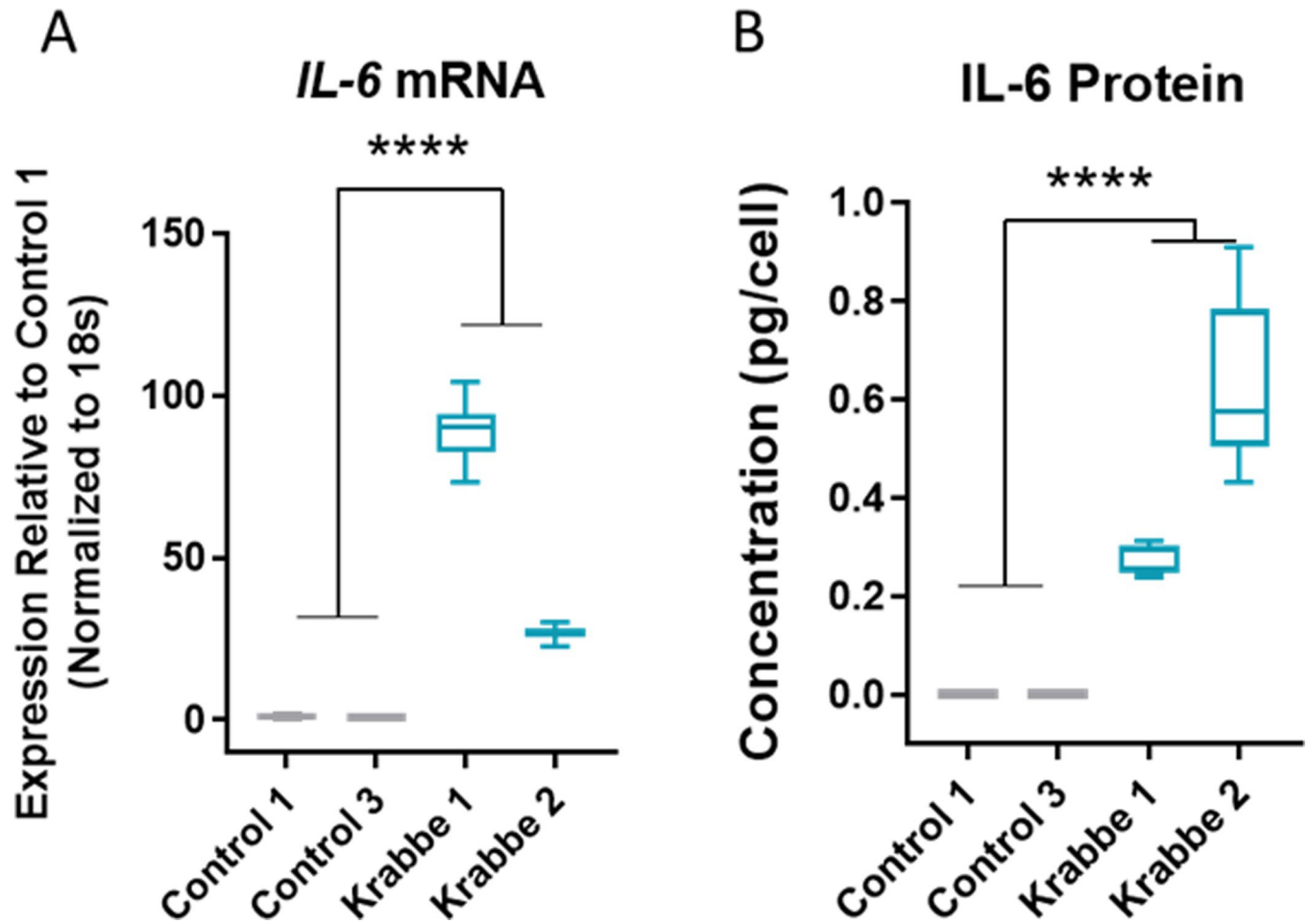


Fig 2. Upregulation of IL-6 in Krabbe astrocytes. Significantly greater IL-6 (A) mRNA and (B) protein expression was observed in astrocytes derived from the donors with Krabbe disease. **** $p < 0.0001$. Data for individual donor subjects is shown as a box and whisker plot with median represented and error bars indicating min/max values. Statistical analysis was conducted using t-tests on pooled data comparing control vs. Krabbe cells.

<https://doi.org/10.1371/journal.pone.0271360.g002>

higher total expression of *IL-6*, *IL-8*, *IL-1 β* , and lower expression of *MCP-1 (CCL2)* than controls following $\text{TNF}\alpha$ stimulation (all adjusted $p < 0.0001$) (S4A–S4D Fig). These findings are consistent with those reported in studies examining mechanisms of disease in human and murine models [20, 21, 32, 59]. In sum, these results validated that Krabbe patient-derived iPSCs were able to be differentiated into $\text{TNF}\alpha$ -responsive astrocytes that recapitulated some key findings of established models of Krabbe disease.

Lipid and gene expression perturbations in Krabbe astrocytes

Lipids in the ceramide metabolic pathway relevant to Krabbe disease were profiled by mass spectroscopy (Fig 3A). Psychosine was detectable and elevated in Krabbe astrocytes compared to undetectable levels in control cells ($t = 11.0$, $p < 0.0001$) (Fig 3B). No significant difference in total galactosylceramide was observed between control and Krabbe astrocytes ($t = 1.6$, $p = 0.14$) (Fig 3C). Examination of specific galactosylceramide isoforms revealed predominant expression of the C16 and C18 chains in our cultures. Krabbe astrocytes had ~2-fold more C16 than controls, while C18 was substantially lower. No other isoforms were robustly detectable (S5 Fig). Total glucosylceramide was significantly elevated in Krabbe astrocytes compared to

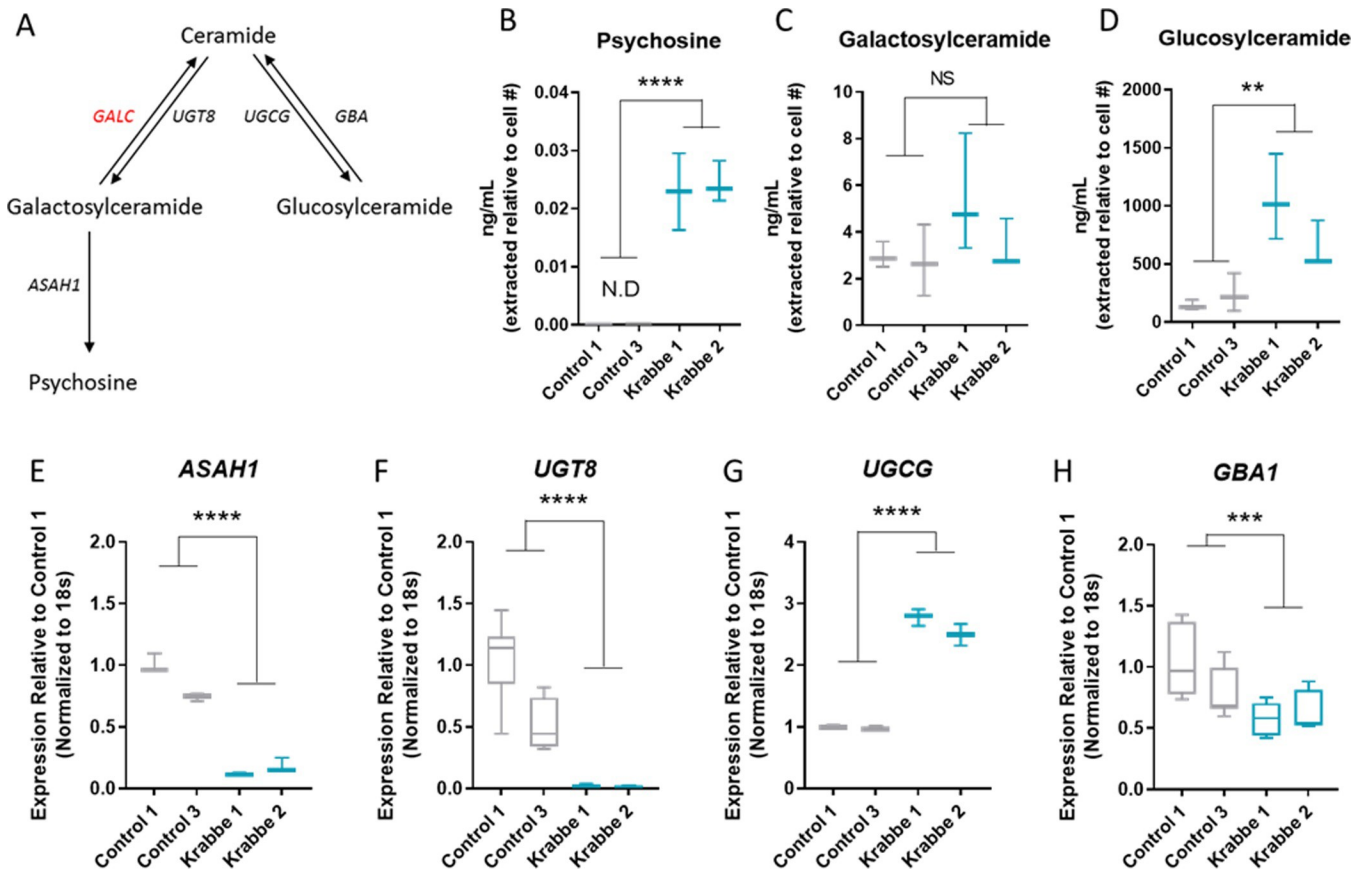


Fig 3. Lipid accumulation and compensatory gene expression changes in Krabbe astrocytes. (A) A simplified schematic of the glycosphingolipid pathway examined in the current study and the genes encoding the enzymes responsible for their biosynthesis. The gene encoding galactosylceramidase (*GALC*), which is defective in Krabbe disease, is indicated in red. (B) Astrocytes generated from the Krabbe donors had significantly elevated levels of psychosine. (C) No significant difference in total non-hydroxylated galactosylceramide was observed between control and Krabbe astrocytes. (D) Increased total non-hydroxylated glucosylceramide was observed in Krabbe astrocytes. (E-H) Compensatory changes in the expression of genes involved in the local glycosphingolipid biosynthesis pathway. For the galactosylceramide arm, a significant downregulation of genes encoding ceramide galactosyltransferase (*UGT8*) and acid ceramidase (*ASAHI*), which are responsible for the biosynthesis of galactosylceramide and psychosine, respectively, was observed in Krabbe astrocytes compared to controls. For the glucosylceramide arm, an upregulation of ceramide glucosyltransferase (*UGCG*) and downregulation of glucocerebrosidase 1 (*GBA1*) was observed in Krabbe astrocytes compared to controls. ** $p < 0.01$, *** $p < 0.001$, **** $p < 0.0001$. Data for individual donor subjects is shown as a box and whisker plot with median represented and errors bars indicating min/max values. Statistical analysis was conducted using t-tests on pooled data comparing control vs. Krabbe cells. N.D. = not detected.

<https://doi.org/10.1371/journal.pone.0271360.g003>

those derived from healthy controls ($t = 4.3$, $p = 0.002$) (Fig 3D). Examination of the specific glucosylceramide isoforms showed this increase was largely driven by longer chain lengths C24:1 and C24 which were ~3-fold higher in Krabbe cells compared to controls. The C16 isoform was also elevated in Krabbe astrocytes, being ~2-fold higher compared to controls (S5 Fig). Hydroxylated galactosylceramide and glucosylceramide were also profiled and were significantly higher in Krabbe astrocytes compared to controls ($t = 3.7$, $p = 0.004$, and $t = 4.3$, $p = 0.002$, respectively). This increase was driven by the C16 isoforms for both hydroxylated lipids, which was the chain length predominantly expressed in our cells (S6A and S6B Fig).

To complement the mass spectroscopy data, we assessed mRNA expression levels of genes encoding lipid biosynthesis enzymes within the galactosylceramide and glucosylceramide metabolic pathways in control and Krabbe astrocytes (Fig 3A). In the galactosylceramide arm of the pathway, Krabbe astrocytes had significantly lower expression of genes encoding acid ceramidase (*ASAHI*, $t = 11.0$, $p < 0.0001$) and ceramide UDP-galactosyltransferase (*UGT8*, $t = 7.0$,

$p < 0.0001$) (Fig 3E and 3F). In the glucosylceramide arm of the pathway, Krabbe astrocytes had significantly higher expression of glucosylceramide synthase (*UGCG*, $t = 18.9$, $p < 0.0001$) and lower expression of glucosylceramidase (*GBA1*, $t = 3.7$, $p = 0.0008$) (Fig 3G and 3H). These results are consistent with the mass spectrometry data described above.

We also measured the concentrations of these lipids in iPSC-derived neurons from the same donor subjects, which were generated as part of the astrocyte differentiation protocol (See [Materials and Methods](#)). We observed significantly elevated psychosine in Krabbe neurons compared to control neurons ($t = 3.5$, $p < 0.01$). There was a slight but significant increase in total non-hydroxylated galactosylceramide in Krabbe neurons ($t = 2.4$, $p = 0.04$), but no significant differences in total hydroxylated galactosylceramide ($t = 1.8$, $p = 0.11$) or non-hydroxylated and hydroxylated glucosylceramide ($t = 1.1$, $p = 0.29$ and $t = 1.0$, $p = 0.34$, respectively) (S7A–S7E Fig). While psychosine levels were relatively similar between Krabbe neurons and astrocytes (S7A Fig), we noted that glucosylceramide (both non-hydroxylated and hydroxylated) levels were substantially higher in Krabbe astrocytes compared to donor-matched neurons (S7D and S7E Fig).

Krabbe astrocytes impact neuron and microglia survival in co-culture

We established co-cultures of astrocytes-neurons and astrocytes-microglia to explore the impact of Krabbe astrocytes on survival of these cell types. Cryopreserved astrocytes were thawed and cultured for 7 days to form a monolayer prior to the seeding of cryopreserved neurons or microglia derived from control donors. The number of HuC/D+ neurons was significantly lower when co-cultured for 96 hours on Krabbe astrocytes compared to control astrocytes (Control 1 neurons: $t = 18.2$, $p < 0.0001$; Control 2 neurons: $t = 30.0$, $p < 0.0001$) (Fig 4A). We observed that dense and complex MAP2+ neuronal projections were able to form over this brief time when neurons were co-cultured with astrocytes derived from control donors. Neurons co-cultured on Krabbe astrocytes appeared clustered and MAP2+ neurites were limited. In contrast, the number of IBA1+ microglia were significantly greater when co-cultured for 96 hours on Krabbe astrocytes compared to control astrocytes (Control 1 microglia: $t = 4.8$, $p < 0.0001$; Control 3 microglia: $t = 8.3$, $p < 0.0001$) (Fig 4B).

As a pilot experiment, we assessed whether direct cell-to-cell contact was needed for the detrimental effect of Krabbe astrocytes on neuronal cell count or if exposure to conditioned media also displayed neurotoxicity. Neuronal medium was conditioned for 96 hours on 3-week-old control and Krabbe astrocyte cultures and then applied to an established monoculture of Control 2 neurons. Following 96 hours of incubation, neuronal viability was significantly lower in cultures containing conditioned media from Krabbe astrocytes compared to neuronal cultures incubated with conditioned medium from control astrocytes ($t = 25.9$, $p < 0.0001$) (S8 Fig).

Substrate reduction approaches fail to rescue neuronal survival

Given the elevated glucosylceramide we observed in the Krabbe astrocytes, we hypothesized that this elevation could be playing a role in their inability to facilitate neuronal survival. Therefore, we explored whether reducing the elevated glucosylceramide in Krabbe astrocytes would rescue the ability of neurons to survive in a co-culture setting. We reduced glucosylceramide by targeting its biosynthetic enzyme, glucosylceramide synthase (GCS), with a proprietary internal GCS inhibitor (S9A Fig). Treatment with 18 nM (corresponding to the IC₉₉) of the GCS inhibitor significantly reduced total non-hydroxylated and hydroxylated glucosylceramide in control and Krabbe astrocytes (adjusted $p < 0.05$ for all lines) (S9B Fig). However, despite a reduction in lipid to non-treated control levels, there was no reduction in basal IL-6

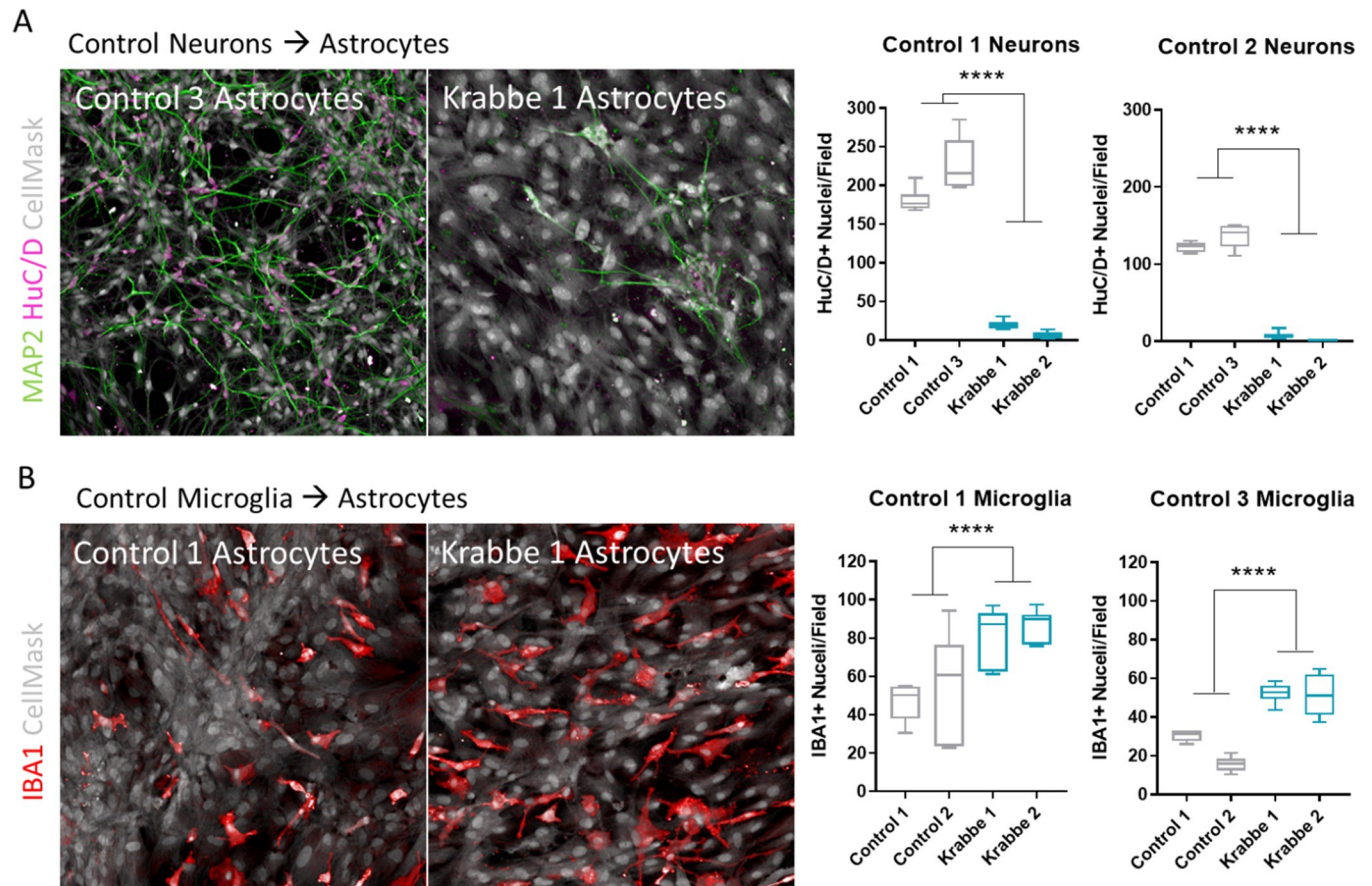


Fig 4. Krabbe astrocytes impact survival of iPSC-derived neurons and microglia in co-culture. Cryopreserved astrocytes from healthy control or Krabbe donors were thawed and cultured for 7 days. Neurons or microglia-like cells generated from two control donors were then seeded onto the established control or Krabbe astrocytes. (A) Representative images of HuC/D positive (purple) and MAP2 positive (green) neurons following 96-hour co-culture with control or Krabbe astrocytes. Significantly fewer HuC/D+ neurons were identified when co-cultured with Krabbe astrocytes. (B) Representative images of IBA1+ (red) microglia following 96-hour co-culture with control or Krabbe astrocytes. A significantly greater number of IBA1+ microglia were identified when co-cultured with Krabbe astrocytes. Representative images in panels A and B were acquired at 20x magnification. **** $p < 0.0001$. Data for individual donor subjects is shown as a box and whisker plot with median represented and errors bars indicating min/max values. Statistical analysis was conducted using t-tests on pooled data comparing control vs. Krabbe cells.

<https://doi.org/10.1371/journal.pone.0271360.g004>

protein expression in supernatant collected from non- $\text{TNF}\alpha$ stimulated Krabbe astrocytes (all adjusted $p > 0.05$) (S9C Fig). To test the effects of astrocytic substrate reduction therapy on neuronal survival, control neurons derived from the Control 2 donor were seeded onto DMSO or GCS inhibitor-treated astrocytes and cultured for 96 hours (S9D Fig). Despite reduced glucosylceramide levels, Krabbe astrocytes negatively impacted neuronal survival, and there was no benefit of glucosylceramide reduction on the number of HuC/D+ nuclei (all $p > 0.05$) (S9E Fig).

Next, we examined whether reducing total sphingolipids in astrocytes would have a beneficial effect on neuronal survival by inhibiting serine palmitoyltransferase (SPTLC1) with Myriocin, which catalyzes the first step in sphingolipid biosynthesis [60] (Fig 5A). 6-day treatment with Myriocin robustly reduced total levels of ceramide, glucosylceramide (both non-hydroxylated and hydroxylated), and galactosylceramide (both non-hydroxylated and hydroxylated) at all concentrations tested (Figs 5B–5D and S10A and S10B). Interestingly, we noted a significant increase in the basal level of ceramide in Krabbe astrocytes compared to control astrocytes (see Fig 5B, average Control vs. Krabbe t-test: $t = 6.6$, $p < 0.001$). Myriocin treatment did not

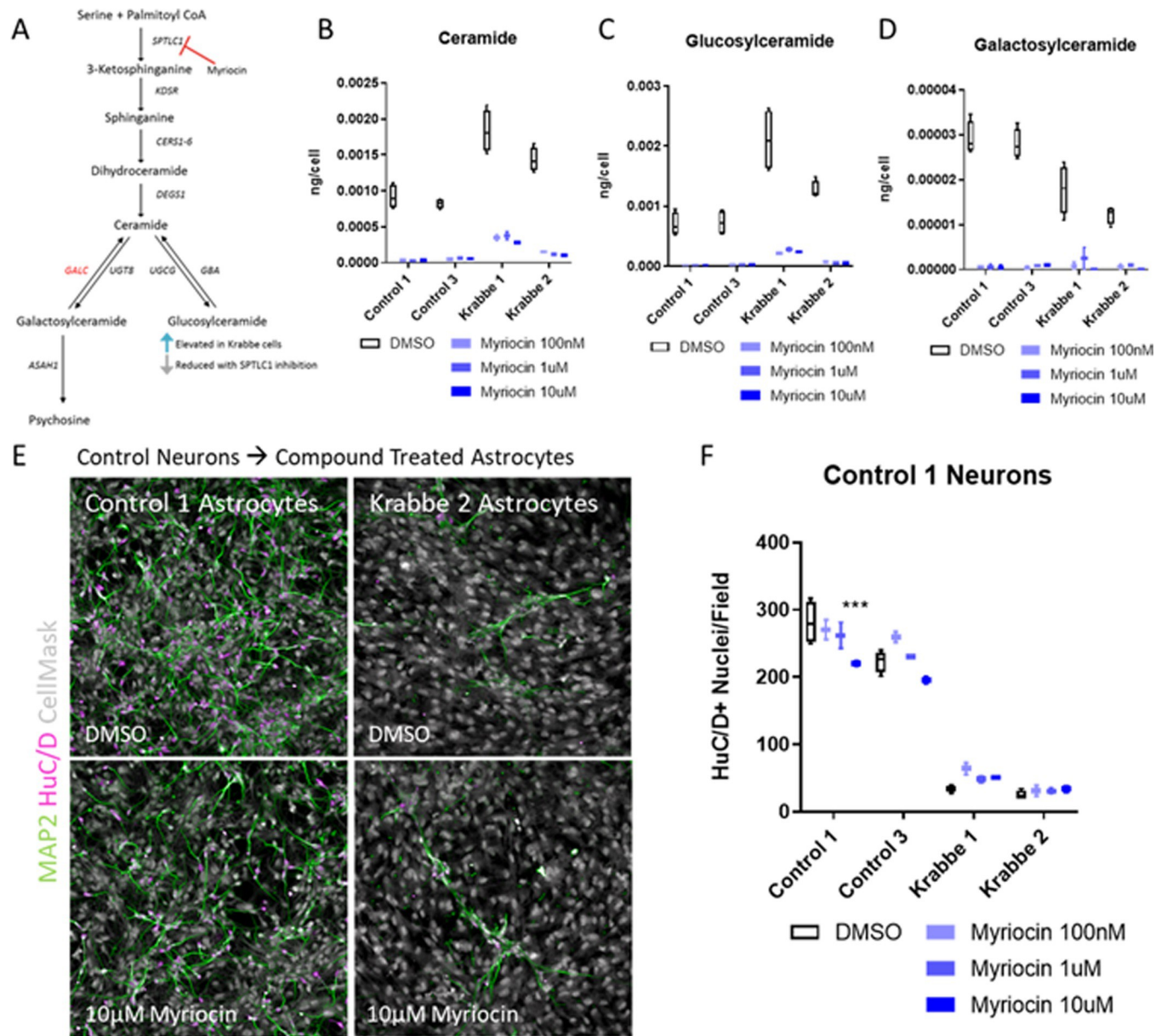


Fig 5. Inhibiting synthesis of ceramide in Krabbe astrocytes fails to facilitate neuronal survival. Cryopreserved astrocytes from healthy control and Krabbe donors were seeded into microwell plates, cultured for 24 hours, and then treated with compound for 6 days prior to analysis. (A) A schematic depicting the biosynthesis of ceramide-derived glycosphingolipids, and the rationale for reducing glucosylceramide via inhibition of SPTLC1 with myriocin. (B-D) Target engagement of myriocin was verified by GC-MS-MS. Myriocin reduced ceramide and its derivatives glucosylceramide and galactosylceramide in control and Krabbe astrocytes. (E, F) Representative images of neuron-astrocyte co-cultures and quantification of the number of HuC/D+ nuclei. No beneficial effect of myriocin was observed when control neurons were co-cultured with Krabbe astrocytes for 72 hours. Data is shown as a box and whisker plot with median represented and errors bars indicating min/max values. *** $p < 0.001$.

<https://doi.org/10.1371/journal.pone.0271360.g005>

reduce psychosine levels in Krabbe astrocytes and in one line was increased following treatment (adjusted $p < 0.05$). This could reflect the inability of Krabbe astrocytes to breakdown psychosine existing prior to treatment. Expression of IL-6 protein in the supernatant of Krabbe astrocytes was unchanged in the Krabbe 1 line at all concentrations and in the Krabbe 2 line at 100 nM (adjusted $p > 0.05$), while slight, but significant, reductions were observed at 1 μ M (adjusted $p = 0.03$) and 10 μ M (adjusted $p = 0.02$) (S11A and S11B Fig). To test the ability of

the myriocin treated Krabbe astrocytes to facilitate neuronal survival in co-culture, neurons derived from the Control 1 donor were co-cultured on compound-treated astrocytes for 72 hours (Fig 5E). Two-way ANOVA revealed no significant effect of Myriocin treatment on the number of HuC/D+ nuclei when co-cultured with Krabbe astrocytes (Fig 5F) (all adjusted $p > 0.05$). We did observe a reduction in HuC/D+ nuclei in the control astrocytes at the highest myriocin concentration tested, which could reflect toxicity of the compound (adjusted $p < 0.001$). In sum, there was a clear and robust effect of Krabbe astrocytes on neuron survival in co-culture, and this was not changed with either GCS or SPTLC1 inhibition despite validation of the expected reduction in downstream sphingolipids.

Discussion

In the current study, we generated iPSC-derived astrocytes from a total of three healthy controls and two donors with infantile onset Krabbe disease and used them to explore phenotypes in disease-relevant cell types. Overall, our findings support and complement a previous report examining iPSCs from Krabbe donors by reproducing observed disease-relevant phenotypes, including psychosine accumulation, impairment of neuronal survival, and perturbation of lipid profiles such as the observation of elevated ceramide [48], as discussed in more detail below. Similar to other reports describing astrocyte differentiation, our iPSC-derived astrocytes from control and Krabbe donors expressed the expected markers vimentin, S100 β , and CD44, and upregulated cytokine gene expression in response to stimulation with TNF α [52, 61]. Importantly, iPSC-derived astrocytes recapitulated many findings observed in humans and in animal models of the disease, including having higher expression of basal IL-6 transcript and protein [31, 59], elevated mRNA expression of *RIPK3* and *MT1E* [57, 58], as well as higher expression of *IL-6*, *IL-1 β* , and *IL-8* and lower expression of *MCP-1 (CCL2)* following stimulation [20, 21, 32, 59]. Perhaps most importantly with respect to the disease state, astrocytes from the Krabbe donors accumulated psychosine, which was undetectable in the control cells [7]. Of note, it has been reported that exogenous application of psychosine in the micromolar range, a level that can be observed in patient samples [7], is toxic to astrocytes *in vitro* [32]. In contrast, our Krabbe iPSC-derived astrocytes appeared morphologically similar and grew as expected compared to healthy control astrocytes. We can only speculate that the endogenous accumulation of psychosine observed in our experiments did not reach the toxic levels required for astrocyte toxicity, which is in concordance with the findings from O'Sullivan and Dev (2015) suggesting that, at optimal density and time of treatment, 10 μ M psychosine treatment is toxic, while 5 μ M does not impact viability [32]. Future experiments might address if longer time in culture would result in astrocyte growth abnormalities or toxicity, or if the endogenous psychosine might "prime" the astrocytes to be more susceptible to an exogenous challenge. In sum, these results imply the validity of using a human iPSC-derived astrocyte model to explore Krabbe disease biology *in vitro*.

A novel finding of our current study was elevated glucosylceramide in the human Krabbe astrocytes. This was accompanied by compensatory changes in gene expression of the enzymes within the local lipid biosynthesis pathway, with lower *UGT8* and *ASAH1* expression, but higher *UGCG* expression, observed in Krabbe astrocytes compared to controls. These findings indicate a shunting away from galactosylceramide and psychosine and towards glucosylceramide (see schematic in Fig 3A). A recent report by Corado and colleagues [62] was the first to identify elevated glucosylceramide in CSF of a canine model of Krabbe disease, which correlated with psychosine and disease progression. They did not observe significant elevation of glucosylceramide in biopsies of the oligodendrocyte-enriched internal capsule or cerebellar white matter, which might suggest that specific cell types are driving the increase observed in

CSF. Although the authors do not examine expression of lipid biosynthesis genes, they speculate in the discussion that broader dysregulation of lysosomal metabolism could lead to a secondary increase in glucosylceramide. The lipid and gene expression results of our study complement their findings and discussion by recapitulating their observed phenotype of elevated glucosylceramide and providing evidence of perturbed dysregulation of the disease-relevant lipid biosynthesis pathway in human cells *in vitro*.

Consistent with the notion of shunting away from the galactosylceramide arm of the pathway, we also observed an increase in total ceramide in Krabbe astrocytes compared to controls. Ceramide has been shown to be elevated in the *twitcher* mouse [63] and in mixed iPSC-derived neural cultures from Krabbe donors [48], providing additional validation of our stem cell model. Furthermore, accumulation of ceramide has been observed in a multitude of degenerative disorders including Alzheimer's [64, 65], Parkinson's [66, 67], and amyotrophic lateral sclerosis [68, 69], among others [70], suggesting that accumulation of ceramide may be a commonality among many neurodegenerative diseases including Krabbe disease. Biologically, ceramide contributes to the regulation of apoptosis [71] and inflammation [72], and in the context of disease, accumulation of ceramide may result in increased susceptibility to apoptosis [73] and enhanced neuroinflammation [74, 75]. To our knowledge, no studies have specifically examined the role of astrocytic ceramide in the pathogenesis of Krabbe disease, but in studies of Alzheimer's disease, aberrant ceramide expression is observed in astrocytes [76], correlates with neuroinflammation [77], and can be secreted in exosomes to influence apoptosis in surrounding cells [78]. With respect to our current study, these results suggest that future research should explore astrocyte-specific sphingolipid metabolism in Krabbe disease. A limitation of the current study is that we did not measure ceramide in the earlier Day 16 neuron cultures, and therefore do not know whether accumulation of ceramide precedes the accumulation of glucosylceramide in Krabbe astrocytes. Taken all together with results of prior studies, our lipid analysis results suggest that the contributions of perturbed sphingolipid biosynthesis to Krabbe disease pathogenesis should continue to be explored.

An exploratory aspect of our study was the in-depth profiling of isoforms of non-hydroxylated and hydroxylated galactosylceramide and glucosylceramide (S5 and S6 Figs) that arise due to various fatty acid chain lengths and hydroxylation state [79]. We observed that shorter chain length (C:16 and C:18) non-hydroxylated galactosylceramides were prominent in our iPSC-derived astrocytes and neurons, with Krabbe astrocytes having ~2 fold higher C:16 galactosylceramide but lower C:18 galactosylceramide compared to controls. C:16, C:24:1, and C:24 non-hydroxylated isoforms of glucosylceramide were all ~2–4 fold higher in Krabbe astrocytes compared to controls, and Krabbe cells also appeared to have a skewed ratio of C:16 to C:18, with higher C:16 and lower C:18 glucosylceramide compared to controls, which appeared to have slightly higher C:18 relative to C:16. The C:16 isoforms of hydroxylated galactosylceramide and glucosylceramide were the predominantly expressed isoforms in cultures from control and Krabbe donors, and were ~2–3 fold higher in Krabbe patient-derived astrocytes. It is worth noting that isoform length and hydroxylation state can affect the glycosphingolipid's hydrophobic properties that result in differences in mobility and membrane localization [10], and that chain length-specific functions [80] and susceptibility to stimuli-induced apoptosis [81] have been observed. It is currently unclear if the shift in chain length to the shorter C:16 isoforms that we observed in the study are important to disease state, and additional work will be needed to understand whether glycosphingolipid chain length and hydroxylation differ in Krabbe patients and if these differences are significant in the context of disease progression.

We next explored the impact of Krabbe astrocytes on survival of neurons and microglia. Co-culturing neurons derived from two control donors onto established monolayers of astrocytes revealed a robust cytotoxic effect of the Krabbe astrocytes, with both Krabbe donor

astrocyte lines negatively impacting the survival of neurons. Our finding is concordant with the results of Mangiameli et al. (2021) that showed a time-dependent reduction in Tuj1+ neurons in mixed neural cultures differentiated from a Krabbe iPSC line [48], although they do not address whether this observed phenotype is related to the astrocytes generated within the cultures through co-culture experiments as explored in our work. Dysfunction of astrocytes has been implicated in the neurodegenerative process for a number of lysosomal storage disorders [82]. For example, specific deletion of *Sumf1*, the gene associated with multiple sulfatase deficiency, in astrocytes induced degeneration of cortical neurons *in vivo* and *in vitro* [83]. Specific deletion of GalC in astrocytes has not been previously done, and given the data presented here such a study would be of interest. We also addressed whether direct cell-to-cell contact was required to observe the neurotoxicity of Krabbe astrocytes by applying astrocyte conditioned media to established neuron mono-cultures. Interestingly, Krabbe astrocyte conditioned media also appeared toxic to neurons, suggesting that, in part, a toxic intermediary is being secreted from Krabbe astrocytes. Notably, other groups have reported that exogenous psychosine exposure is toxic to human and murine neurons [22, 25]. Therefore, it is possible that in our system the psychosine accumulated in Krabbe astrocytes is in part secreted into the media and contributes to the observed neuronal toxicity. Alternatively, proteins secreted by Krabbe astrocytes, such as inflammatory cytokines may impact neuronal survival. Future proteomic or lipidomic studies examining the supernatant of Krabbe astrocytes may yield interesting information explaining the observed neurotoxicity and identify new targets for therapeutic intervention.

In stark contrast to the finding of cytotoxicity to neurons, we observed a greater number of control donor-derived microglia when co-cultured with Krabbe astrocytes compared to control astrocytes. The mechanisms as to how Krabbe astrocytes contributed to the increased number of microglia in our culture model was not the focus of the current studies, but the effect may be mediated by release of factors beneficial to microglial survival from astrocytes and/or influence via direct cell-to-cell interactions. As a proof-of-concept example, Takata et al., (2017) show that both co-culture with neurons or culture with neuron conditioned media is beneficial to iPSC-derived microglia survival, with direct co-culture being the most beneficial [84]. In this study we did not examine whether the beneficial effect of co-culture with Krabbe astrocytes on microglial survival required cell-cell contact or could be recapitulated with astrocyte-conditioned media alone. We also have not performed microglia-neuronal co-cultures, as this was beyond the scope of the current study, which focused on the role of Krabbe astrocytes. Microglia have been implicated in exacerbating the pathogenesis of Krabbe disease via mechanisms including promoting neuroinflammation and by the abnormal phagocytosis of myelin debris [85–87], and evidence suggests that microglia are the origin of the disease-namesake multinucleated globoid cells that appear around areas of demyelination [28, 29, 88]. To this end, psychosine-stimulated astrocytes release matrix metalloproteinase-3 (MMP-3) that has been shown to drive the formation of microglia into globoid cells [28], suggesting that cross talk between astrocytes and microglia are central to Krabbe disease.

It is important to address that an increased number of microglia might be beneficial in the setting of disease, and therefore the mechanisms leading to increased number of microglia in our culture system could provide insights into possible therapeutics. Alami et al. (2018) elegantly showed that astrocyte activation of NF- κ B signaling promotes microglial proliferation in the SOD1 mutant mouse model of amyotrophic lateral sclerosis, which was beneficial in the early stages of disease by delaying onset of symptoms, but turned detrimental in the later stages of disease by accelerating disease progression [89]. The biphasic benefit of increased number of microglia was accompanied by a switch in microglia state, from an anti-inflammatory M2 state early in disease to a pro-inflammatory M1 state in the later stages [89]. In the context of

Krabbe disease, Kondo et al. (2011) addressed the question as to whether the presence of microglia are beneficial by crossing the *twitcher* mouse with the macrophage deficient osteopetrotic mutant mouse, resulting in substantially fewer microglia and macrophages in the brain [90]. Results from their studies suggested that the lack of microglia accelerated disease progression, exacerbated disease phenotypes, and led to increased myelin debris in the white matter and impaired remyelination in the spinal cord [90]. Findings from these reports suggest that increased numbers of anti-inflammatory microglia may be beneficial in curbing disease progression. Therefore, it is possible that Krabbe astrocytes secrete factors that support microglia, thus reflecting their potential protective role. Future studies should aim to study the reactive state of microglia co-cultured with Krabbe astrocytes, as it may yield important insights into how astrocyte-microglia interactions are related to Krabbe disease pathogenesis.

In our final experiments, we addressed whether reduction of the elevated sphingolipids in Krabbe astrocytes had a beneficial effect on neuronal survival in co-culture. We show that small molecules can substantially reduce the accumulation of ceramide and glucosylceramide in Krabbe astrocytes, although we did not observe any benefit of these inhibitors on the number of neurons when co-cultured with Krabbe astrocytes. While we did not examine psychosine level in the GCS inhibitor experiment, as we would not expect a reduction with this compound, we did observe that psychosine levels were not reduced in Krabbe astrocytes following myriocin treatment. We would predict that inhibiting the ceramide biosynthesis pathway would reduce psychosine, or at least prevent further accumulation, by reducing the availability of its precursor galactosylceramide. Our result suggests that the psychosine present in the Krabbe cultures prior to myriocin treatment remains in the cells, as it is unable to be degraded due to deficiency in GALC, a protective function under normal conditions [7]. This is supported by the observation that the levels of psychosine don't appear to further increase in the Day ~63 Krabbe astrocytes compared to their earlier Day 16 neuronal precursors (see S7 Fig). The changes we observed in gene expression of enzymes in the lipid biosynthesis pathway and the subsequent shunting away from psychosine towards glucosylceramide in Krabbe astrocytes, but not neurons, might be a compensatory mechanism that manifests over time in culture to limit the additional accumulation of psychosine. Together these data imply that substrate reduction approaches should target psychosine synthesis directly, and early in the disease state, rather than perturbations related to compensatory mechanisms. Indeed, recent evidence shows that inhibition of acid ceramidase, either genetically or with a small molecule, provides benefit on the survival of the Krabbe *twitcher* murine model [91]. Two reports have examined novel UGT8 inhibitors to block synthesis of psychosine precursor galactosylceramide, and showed reduction of brain psychosine, beneficial effects on neuroinflammation phenotypes, and extension of lifespans in Krabbe *twitcher* mice [92, 93]. Furthermore, studies using L-cycloserine, a serine palmitoyltransferase inhibitor, have shown benefit on survival and disease phenotypes in the *twitcher* model, but only when the compound is administered before the onset of symptoms [94, 95]. In the context of our findings, earlier treatment with myriocin might prove efficacious in our co-culture model if it were added prior to psychosine accumulation.

While our substrate reduction approach complements the strategies of the publications highlighted above, it is important to put our results in the context of reports suggesting that modulation of the sphingolipid pathway that is perturbed by GALC deficiency could be efficacious in the setting of Krabbe disease. Sphingosine-1-phosphate, a bioactive molecule within the sphingolipid metabolic pathway, signals through G-protein coupled receptors located on numerous cell types on the central and immune systems, and regulates diverse biological functions including apoptosis, cell growth, and inflammation, among others [32, 96, 97]. Agonism of the sphingosine-1-phosphate receptor (S1PR) with Fingolimod (FTY720) attenuated

psychosine-induced cell death in cultured human astrocytes [32], psychosine-induced demyelination in mouse organotypic slice cultures [33] and importantly ameliorated demyelination, restored astrocyte and microglial reactivity, and extended lifespan in Krabbe *twitcher* mice [98]. The authors highlight that the beneficial effects of Fingolimod in Krabbe models could, in part, be mediated by its ability to modulate astrocyte reactivity and inflammatory cytokine release [32, 98]. With respect to our findings, we report that substrate reduction strategies targeting glucosylceramide accumulation did not produce robust changes in IL-6 levels in Krabbe astrocytes, which might suggest that we are not altering the inflammatory profile of these cells, and in the context of the findings discussed, could be related to our lack of treatment effect on the number of HuC/D+ neurons quantified in co-cultures. Further examining of the astrocyte inflammatory response by profiling additional cytokines would be helpful to answer the question of how broadly we are impacting their state. Furthermore, a future experiment could directly compare modulation of the S1PR to the substrate reduction approaches mentioned using our described phenotype in astrocyte-neuron co-cultures.

The results of our study need to be considered with respect to its limitations, in addition to those noted above. First, we only examined astrocytes generated from donors with infantile onset Krabbe disease, and both donors were homozygous for the large ~30 kb deletion in *GALC* found in Caucasians that results in near complete loss of enzyme activity [49]. Therefore, it is unclear as to whether astrocytes generated from donors harboring other disease-causing mutations, including those resulting in less severe later-onset forms of the disease, would display the same phenotypes identified in our study. Accordingly, it is challenging to interpret instances of between-line variability that we observed in some phenotypes, including IL-6 expression or psychosine levels following compound treatment, and it remains unclear whether these differences represent heterogeneity in patient phenotypes or *in vitro* assay artifacts. Examination of additional Krabbe lines will help elucidate the most relevant biological phenotypes in these cells. Indeed, the recent report examining differentiation of Krabbe donor iPSCs presented differences in lipidomic profiles and differentiation potential in patient lines with different mutations [48], highlighting the importance of profiling additional donor backgrounds. Second, we did not examine whether correcting expression of *GALC* in Krabbe astrocytes, perhaps by lentiviral-mediated overexpression of the gene in stem cells [99, 100] and subsequent differentiation into astrocyte lineage, would reverse the psychosine, ceramide, and glucosylceramide accumulation, compensatory expression changes in lipid synthesizing genes, and cytotoxicity to co-cultured neurons observed in our study. Without the *GALC* corrected cell lines it is difficult to interpret whether our findings are caused directly by deficient activity of *GALC* or compensatory changes in other enzymes. Third, while we assessed lipid accumulation in Krabbe neuronal cultures and noted psychosine accumulation, we did not further probe whether disease-related phenotypes could be observed in Krabbe neurons alone, as this was not the aim of the current study. However, others have noted neuron-specific phenotypes in neurons derived from human Krabbe donors [25] and the *twitcher* mouse [24, 27]. It would be of interest to explore how co-culture of Krabbe neurons with control astrocytes would behave, and if any defects observed in Krabbe neurons (for example, psychosine accumulation) could be corrected by co-culture with control astrocytes. Finally, we only explored perturbations in the lipid biosynthesis pathway directly surrounding psychosine. A multi-omics approach examining transcriptomic, lipidomic, and proteomic changes in Krabbe astrocytes would yield valuable insight into broad changes that might occur in disease-relevant cell types and offer novel targets for therapeutic interventions.

In conclusion, we show that astrocytes derived from Krabbe donors recapitulated many reported findings from human and rodent studies. We were able to uncover phenotypes relevant to the disease, including perturbed lipid biosynthesis and differential effects on neuron

and microglia survival. Our results complement previous publications and further suggest that the contribution of astrocytes to the pathogenesis of Krabbe disease warrants further investigation.

Supporting information

S1 Fig. Validation of the large deletion within *GALC* in Krabbe fibroblasts. Prior to reprogramming, the ~30 kB deletion within *GALC* was confirmed in fibroblasts via qPCR by applying TaqMan selected probe and primer sets spanning specific exons. As expected, mRNA was detected using a probe spanning exons 3–4 in control and Krabbe fibroblasts. No detectable message was observed using probes spanning exons 13–14, 14–15, or 15–16, consistent with the deletion between exons 11–17 reported by the Coriell biobank.

(DOCX)

S2 Fig. Qualitative assessment of Krabbe iPSCs ability to differentiate into neural cultures. Immunocytochemistry was used to assess the neural differentiation potential of Krabbe iPSCs prior to expansion and differentiation to astrocytes. *Top row:* No robust difference was observed in Krabbe iPSCs to generate cultures containing HuC/D+ (green) neurons and SOX2+ (orange) neural progenitors. *Middle row:* Control and Krabbe neural cultures contained Tuj1+ (green) neurites. A minor portion of the neurons in each of the cultures expressed dopaminergic-marker tyrosine hydroxylase (TH, orange). *Bottom row:* MAP2+ (orange) neurites were observed in control and Krabbe cultures. In all images, nuclei are counterstained with Hoechst and visualized in blue.

(DOCX)

S3 Fig. Upregulation of *RIPK3* and *MT1E* in Krabbe astrocytes recapitulates findings in humans and in animal models of the disease. Basal expression of *RIPK3* and *MT1E* mRNA was upregulated in Krabbe astrocytes. These results are in line with published findings in human and rodent data sets showing elevated transcript expression in Krabbe disease. Data for individual donor subjects is shown as a box and whisker plot with median represented and errors bars indicating min/max values. Statistical analysis was conducted using t-tests on pooled data comparing control vs. Krabbe cells. **** $p < 0.0001$.

(DOCX)

S4 Fig. mRNA expression of *IL-6*, *IL-8*, *IL-1 β* , and *MCP-1 (CCL2)* following TNF α stimulation. Astrocytes from 2 healthy control donors and 2 Krabbe donors stimulated with 50 ng/mL TNF α for 24 hours. Significant effects with TNF α treatment, donor genotype, and interactions between the two were observed. TNF α treatment induced upregulation of mRNA levels of the four gene examined. Post-hoc analysis comparing expression following TNF α treatment revealed higher expression of *IL-6*, *IL-8*, and *IL-1 β* , and lower expression of *MCP-1 (CCL2)* in Krabbe donors. Data for individual donor subjects is shown as a box and whisker plot with median represented and errors bars indicating min/max values, and is visualized relative to the mock condition of Control cells. Statistics were performed using two-way ANOVA with post-hoc test comparing expression values following TNF treatment. *** $p < 0.001$, **** $p < 0.0001$.

(DOCX)

S5 Fig. Non-hydroxylated galactosylceramide and glucosylceramide species in iPSC-derived astrocytes. (A) The profile of non-hydroxylated galactosylceramide species in control and Krabbe astrocytes suggests that shorter carbon chain length species are the predominant isoforms. While no difference in total non-hydroxylated galactosylceramide was found (see

Fig 2C), examination of the specific isoforms shows that the C16 species was elevated in Krabbe astrocytes, but the C18 isoform was more specific to control astrocytes. (B) The profile of non-hydroxylated glucosylceramide in control and Krabbe astrocytes suggests that the elevated levels of total glucosylceramide observed in Krabbe astrocytes is being driven by the short C16 and long C24:1 and C24 isoforms. Data showing isoform expression is depicted as mean \pm SD.

(DOCX)

S6 Fig. Hydroxylated (OH) galactosylceramide and glucosylceramide species in iPSC-derived astrocytes. (A) Hydroxylated galactosylceramide was higher in Krabbe astrocytes compared to controls. Examination of the species of OH-galactosylceramide expressed in our cell cultured revealed this increase was driven by C16 OH-galactosylceramide. (B) Hydroxylated glucosylceramide was significantly higher in Krabbe astrocytes compared to controls. This increase was also driven by C16 OH-glucosylceramide, which was the predominant isoform expressed in iPSC-derived astrocytes. Data for individual donor subjects is shown as a box and whisker plot with median represented and errors bars indicating min/max values. Data showing isoform expression is depicted as mean \pm SD. Statistical analysis was conducted using t-tests on pooled data comparing control vs. Krabbe cells. ** $p < 0.01$.

(DOCX)

S7 Fig. Comparison of total psychosine, galactosylceramide, and glucosylceramide lipid levels in iPSC-derived neuron and astrocyte mono-cultures from control and Krabbe donors. Cryopreserved neurons from 2 control and 2 Krabbe donors were seeded and cultured for 7 days prior to lipid analysis. Data and statistical significance from astrocytes is shown for comparison, and is identical to the data depicted in Fig 3. Astrocytes were generated from extended culture (~63–65 days) of the same neuronal cells. (A) Significantly elevated psychosine was detected in Krabbe neurons compared to Control neurons, where it was below the level of detection ($t = 3.5$, $p = 0.007$). The level of psychosine appeared comparable in Krabbe neurons and astrocytes. (B) A slight, but significant, elevation in non-hydroxylated galactosylceramide was observed in Krabbe neurons ($t = 2.4$, $p = 0.04$). (C-E) No significant differences were observed between control and Krabbe neurons in OH-galactosylceramide, glucosylceramide, or OH-glucosylceramide. Interestingly, both non-hydroxylated and hydroxylated glucosylceramide levels were substantially higher in Krabbe astrocytes compared to Krabbe neurons. Data for individual donor subjects is shown as a box and whisker plot with median represented and errors bars indicating min/max values. Statistical analysis was conducted using t-tests on pooled data comparing control vs. Krabbe cells. NS = not significant, * $p < 0.05$, ** $p < 0.01$, *** $p < 0.001$.

(DOCX)

S8 Fig. Conditioned media from Krabbe astrocytes impedes neuronal survival. Neuronal media was conditioned on astrocytes from control and Krabbe donors for 7 days prior to being transferred onto already established neuron cultures from a healthy control donor for 96 hours. The live and dead cell fluorescent probes Calcein Green AM and NucRed Dead were used to quantify viability relative to the total number of nuclei identified via Hoechst staining (Note: Hoechst is not shown in the images). Quantification of the percent of live cells revealed a significant reduction when neurons were cultured in Krabbe astrocyte conditioned medium ($p < 0.0001$). Data was obtained from neurons grown in a 384 well plate, with 64 wells used for each conditioned media group. Data for individual donor subjects is shown as a box and whisker plot with median represented and errors bars indicating min/max values. Statistical analysis was conducted using t-tests on pooled data comparing control vs. Krabbe cells. ****

$p < 0.0001$.
(DOCX)

S9 Fig. Glucosylceramide synthase inhibition fails to rescue neuronal survival when co-cultured with Krabbe astrocytes. Astrocytes were thawed into 96 well assay plates. The following day media was replaced with fresh astrocyte media containing 18 nM (IC99) of an in-house glucosylceramide synthase inhibitor. Fresh media and compound were replaced every 3 days. After 9 days of treatment, cells were either harvested for lipid analysis via LC-MS-MS and IL-6 protein expression analysis via alphaLISA or used for a co-culture assay by seeding control neurons in neuronal media supplemented with GCS inhibitor for an additional 96 hours. (A-B) A simplified schematic of the ceramide biosynthetic pathway indicates the rationale for the experiment. Target engagement was validated following 9-day inhibition of GCS by the reduced levels of glucosylceramide and OH-glucosylceramide in the astrocyte cultures, including a substantial reduction in the Krabbe cells to near untreated healthy control levels. (C) IL-6 protein expression was not reduced in the astrocytes following GCS inhibitor treatment. (D-E) Co-culture of healthy control neurons with Krabbe astrocytes revealed no beneficial effect of GCS inhibition on neuronal survival. Data for individual donor subjects is shown as a box and whisker plot with median represented and errors bars indicating min/max values. Statistical analysis was determined as adjusted $p < 0.05$ and conducted using Two-way ANOVA with Bonferroni post hoc test comparing DMSO vs compound treated samples. ** $p < 0.01$, *** $p < 0.001$.
(DOCX)

S10 Fig. Effects of SPTLC1 inhibition effects on OH-GlcCer and OH-GalCer in astrocytes. 6-day treatment with Myriocin reduced levels of hydroxylated (A) glucosylceramide and (B) galactosylceramide at all concentrations examined in iPSC-derived astrocytes from control and Krabbe donors. Data is shown as a box and whisker plot with median represented and errors bars indicating min/max values.
(DOCX)

S11 Fig. SPTLC1 inhibition does not reduce Psychosine or IL-6 expression in Krabbe astrocytes. (A) 6-day treatment with Myriocin did not reduce Psychosine in Krabbe astrocytes. No change was observed in Krabbe 2 astrocytes. A significant upregulation was observed at the two lowest concentrations in Krabbe 1 astrocytes. (B) No significant change in IL-6 protein was detected in the supernatant of Krabbe 1 astrocytes treated with Myriocin, while slight, but significant reduction was seen at the 1 μM and 10 μM concentrations in Krabbe 2 astrocytes. Data is shown as a box and whisker plot with median represented and errors bars indicating min/max values. * $p < 0.05$, ** $p < 0.01$, **** $p < 0.0001$.
(DOCX)

Acknowledgments

We would like to acknowledge Dr. Cecile Orsini, Dr. Dorine Chassin, Nicolas Bodier, and Nicole Meritet from the Translational Sciences unit at Sanofi for their assistance with the protocols for iPSC culture and NPC differentiation.

Author Contributions

Conceptualization: Richard Lieberman, Leslie K. Cortes, Patrick L. Jones.

Data curation: Richard Lieberman, Grace Gao, Hyejung Park.

Formal analysis: Richard Lieberman, Leslie K. Cortes, Grace Gao, Hyejung Park.

Supervision: Leslie K. Cortes, Bing Wang, Patrick L. Jones, R. Bridge Hunter, John P. Leonard, Robert H. Barker, Jr.

Writing – original draft: Richard Lieberman, Leslie K. Cortes, Hyejung Park.

Writing – review & editing: Leslie K. Cortes, Grace Gao, Hyejung Park, Bing Wang, Patrick L. Jones, R. Bridge Hunter, John P. Leonard, Robert H. Barker, Jr.

References

1. Suzuki K, Suzuki Y. Globoid cell leucodystrophy (Krabbe's disease): deficiency of galactocerebroside beta-galactosidase. *Proc Natl Acad Sci U S A*. 1970; 66(2):302–9. Epub 1970/06/01. <https://doi.org/10.1073/pnas.66.2.302> PMID: 5271165; PubMed Central PMCID: PMC283044.
2. Kohlschutter A. Lysosomal leukodystrophies: Krabbe disease and metachromatic leukodystrophy. *Handb Clin Neurol*. 2013; 113:1611–8. Epub 2013/04/30. <https://doi.org/10.1016/B978-0-444-59565-2.00029-0> PMID: 23622382.
3. Jesionek-Kupnicka D, Majchrowska A, Krawczyk J, Wendorff J, Barcikowska M, Lukaszek S, et al. Krabbe disease: an ultrastructural study of globoid cells and reactive astrocytes at the brain and optic nerves. *Folia Neuropathol*. 1997; 35(3):155–62. Epub 1997/01/01. PMID: 9595850.
4. Wenger DA. Research update on lysosomal disorders with special emphasis on metachromatic leukodystrophy and Krabbe disease. *APMIS Suppl*. 1993; 40:81–7. Epub 1993/01/01. PMID: 8311994.
5. Wenger DA, Rafi MA, Luzi P, Datto J, Costantino-Ceccarini E. Krabbe disease: genetic aspects and progress toward therapy. *Mol Genet Metab*. 2000; 70(1):1–9. Epub 2000/06/02. <https://doi.org/10.1006/mgme.2000.2990> PMID: 10833326.
6. Zlotogora J, Chakraborty S, Knowlton RG, Wenger DA. Krabbe disease locus mapped to chromosome 14 by genetic linkage. *Am J Hum Genet*. 1990; 47(1):37–44. Epub 1990/07/01. PMID: 1971996; PubMed Central PMCID: PMC1683747.
7. Svennerholm L, Vanier MT, Mansson JE. Krabbe disease: a galactosylsphingosine (psychosine) lipidoses. *J Lipid Res*. 1980; 21(1):53–64. Epub 1980/01/01. PMID: 7354254.
8. Schulze H, Sandhoff K. Sphingolipids and lysosomal pathologies. *Biochim Biophys Acta*. 2014; 1841(5):799–810. Epub 2013/11/05. <https://doi.org/10.1016/j.bbailip.2013.10.015> PMID: 24184515.
9. Suzuki K. Twenty five years of the "psychosine hypothesis": a personal perspective of its history and present status. *Neurochem Res*. 1998; 23(3):251–9. Epub 1998/03/03. <https://doi.org/10.1023/a:1022436928925> PMID: 9482237.
10. Spassieva S, Bieberich E. Lysosphingolipids and sphingolipidoses: Psychosine in Krabbe's disease. *J Neurosci Res*. 2016; 94(11):974–81. Epub 2016/09/18. <https://doi.org/10.1002/jnr.23888> PMID: 27638582; PubMed Central PMCID: PMC5027979.
11. Guenzel AJ, Turgeon CT, Nickander KK, White AL, Peck DS, Pino GB, et al. The critical role of psychosine in screening, diagnosis, and monitoring of Krabbe disease. *Genet Med*. 2020. Epub 2020/02/25. <https://doi.org/10.1038/s41436-020-0764-y> PMID: 32089546.
12. Escolar ML, Kiely BT, Shawgo E, Hong X, Gelb MH, Orsini JJ, et al. Psychosine, a marker of Krabbe phenotype and treatment effect. *Mol Genet Metab*. 2017; 121(3):271–8. Epub 2017/06/06. <https://doi.org/10.1016/j.ymgme.2017.05.015> PMID: 28579020; PubMed Central PMCID: PMC5548593.
13. Folts CJ, Scott-Hewitt N, Proschel C, Mayer-Proschel M, Noble M. Lysosomal Re-acidification Prevents Lysosphingolipid-Induced Lysosomal Impairment and Cellular Toxicity. *PLoS Biol*. 2016; 14(12):e1002583. Epub 2016/12/16. <https://doi.org/10.1371/journal.pbio.1002583> PMID: 27977664; PubMed Central PMCID: PMC5169359.
14. White AB, Givogri MI, Lopez-Rosas A, Cao H, van Breemen R, Thinakaran G, et al. Psychosine accumulates in membrane microdomains in the brain of krabbe patients, disrupting the raft architecture. *J Neurosci*. 2009; 29(19):6068–77. Epub 2009/05/15. <https://doi.org/10.1523/JNEUROSCI.5597-08.2009> PMID: 19439584; PubMed Central PMCID: PMC6665501.
15. Hawkins-Salsbury JA, Parameswar AR, Jiang X, Schlesinger PH, Bongarzone E, Ory DS, et al. Psychosine, the cytotoxic sphingolipid that accumulates in globoid cell leukodystrophy, alters membrane architecture. *J Lipid Res*. 2013; 54(12):3303–11. Epub 2013/09/06. <https://doi.org/10.1194/jlr.M039610> PMID: 24006512; PubMed Central PMCID: PMC3826678.
16. Hannun YA, Bell RM. Lysosphingolipids inhibit protein kinase C: implications for the sphingolipidoses. *Science*. 1987; 235(4789):670–4. Epub 1987/02/06. <https://doi.org/10.1126/science.3101176> PMID: 3101176

17. Giri S, Khan M, Rattan R, Singh I, Singh AK. Krabbe disease: psychosine-mediated activation of phospholipase A2 in oligodendrocyte cell death. *J Lipid Res.* 2006; 47(7):1478–92. Epub 2006/04/29. <https://doi.org/10.1194/jlr.M600084-JLR200> PMID: 16645197.
18. Misslin C, Velasco-Estevez M, Albert M, O'Sullivan SA, Dev KK. Phospholipase A2 is involved in galactosylsphingosine-induced astrocyte toxicity, neuronal damage and demyelination. *PLoS One.* 2017; 12(11):e0187217. Epub 2017/11/03. <https://doi.org/10.1371/journal.pone.0187217> PMID: 29095858; PubMed Central PMCID: PMC5667767.
19. Haq E, Giri S, Singh I, Singh AK. Molecular mechanism of psychosine-induced cell death in human oligodendrocyte cell line. *J Neurochem.* 2003; 86(6):1428–40. Epub 2003/09/03. <https://doi.org/10.1046/j.1471-4159.2003.01941.x> PMID: 12950451.
20. Formichi P, Radi E, Battisti C, Pasqui A, Pompella G, Lazzarini PE, et al. Psychosine-induced apoptosis and cytokine activation in immune peripheral cells of Krabbe patients. *J Cell Physiol.* 2007; 212(3):737–43. Epub 2007/04/27. <https://doi.org/10.1002/jcp.21070> PMID: 17458901.
21. Giri S, Jatana M, Rattan R, Won JS, Singh I, Singh AK. Galactosylsphingosine (psychosine)-induced expression of cytokine-mediated inducible nitric oxide synthases via AP-1 and C/EBP: implications for Krabbe disease. *FASEB J.* 2002; 16(7):661–72. Epub 2002/04/30. <https://doi.org/10.1096/fj.01-0798com> PMID: 11978730.
22. Sugama S, Kim SU, Ida H, Eto Y. Psychosine cytotoxicity in rat neural cell cultures and protection by phorbol ester and dimethyl sulfoxide. *Pediatr Res.* 1990; 28(5):473–6. Epub 1990/11/01. <https://doi.org/10.1203/00006450-199011000-00011> PMID: 2255570.
23. Suzuki K. Globoid cell leukodystrophy (Krabbe's disease): update. *J Child Neurol.* 2003; 18(9):595–603. Epub 2003/10/24. <https://doi.org/10.1177/08830738030180090201> PMID: 14572137.
24. Castelvetti LC, Givogri MI, Zhu H, Smith B, Lopez-Rosas A, Qiu X, et al. Axonopathy is a compounding factor in the pathogenesis of Krabbe disease. *Acta Neuropathol.* 2011; 122(1):35–48. Epub 2011/03/05. <https://doi.org/10.1007/s00401-011-0814-2> PMID: 21373782; PubMed Central PMCID: PMC3690521.
25. Lim SM, Choi BO, Oh SI, Choi WJ, Oh KW, Nahm M, et al. Patient fibroblasts-derived induced neurons demonstrate autonomous neuronal defects in adult-onset Krabbe disease. *Oncotarget.* 2016; 7(46):74496–509. Epub 2016/10/27. <https://doi.org/10.18632/oncotarget.12812> PMID: 27780934; PubMed Central PMCID: PMC5342682.
26. Cantuti Castelvetti L, Givogri MI, Hebert A, Smith B, Song Y, Kaminska A, et al. The sphingolipid psychosine inhibits fast axonal transport in Krabbe disease by activation of GSK3beta and deregulation of molecular motors. *J Neurosci.* 2013; 33(24):10048–56. Epub 2013/06/14. <https://doi.org/10.1523/JNEUROSCI.0217-13.2013> PMID: 23761900; PubMed Central PMCID: PMC3682375.
27. Smith BR, Santos MB, Marshall MS, Cantuti-Castelvetti L, Lopez-Rosas A, Li G, et al. Neuronal inclusions of alpha-synuclein contribute to the pathogenesis of Krabbe disease. *J Pathol.* 2014; 232(5):509–21. Epub 2014/01/15. <https://doi.org/10.1002/path.4328> PMID: 24415155; PubMed Central PMCID: PMC3977150.
28. Ijichi K, Brown GD, Moore CS, Lee JP, Winokur PN, Pagarigan R, et al. MMP-3 mediates psychosine-induced globoid cell formation: implications for leukodystrophy pathology. *Glia.* 2013; 61(5):765–77. Epub 2013/02/14. <https://doi.org/10.1002/glia.22471> PMID: 23404611; PubMed Central PMCID: PMC3804069.
29. Claycomb KI, Winokur PN, Johnson KM, Nicaise AM, Giampetruzzi AW, Sacino AV, et al. Aberrant production of tenascin-C in globoid cell leukodystrophy alters psychosine-induced microglial functions. *J Neuropathol Exp Neurol.* 2014; 73(10):964–74. Epub 2014/09/06. <https://doi.org/10.1097/NEN.000000000000117> PMID: 25192051; PubMed Central PMCID: PMC4169335.
30. Scott-Hewitt NJ, Folts CJ, Noble MD. Heterozygous carriers of galactocerebrosidase mutations that cause Krabbe disease have impaired microglial function and defective repair of myelin damage. *Neural Regen Res.* 2018; 13(3):393–401. Epub 2018/04/07. <https://doi.org/10.4103/1673-5374.228712> PMID: 29623914; PubMed Central PMCID: PMC5900492.
31. Snook ER, Fisher-Perkins JM, Sansing HA, Lee KM, Alvarez X, MacLean AG, et al. Innate immune activation in the pathogenesis of a murine model of globoid cell leukodystrophy. *Am J Pathol.* 2014; 184(2):382–96. Epub 2013/12/10. <https://doi.org/10.1016/j.ajpath.2013.10.011> PMID: 24316110; PubMed Central PMCID: PMC3906490.
32. O'Sullivan C, Dev KK. Galactosylsphingosine (psychosine)-induced demyelination is attenuated by sphingosine 1-phosphate signalling. *J Cell Sci.* 2015; 128(21):3878–87. Epub 2015/09/12. <https://doi.org/10.1242/jcs.169342> PMID: 26359302.
33. O'Sullivan C, Schubart A, Mir AK, Dev KK. The dual S1PR1/S1PR5 drug BAF312 (Siponimod) attenuates demyelination in organotypic slice cultures. *J Neuroinflammation.* 2016; 13:31. Epub 2016/02/10. <https://doi.org/10.1186/s12974-016-0494-x> PMID: 26856814; PubMed Central PMCID: PMC4746808.

34. Giri S, Khan M, Nath N, Singh I, Singh AK. The role of AMPK in psychosine mediated effects on oligodendrocytes and astrocytes: implication for Krabbe disease. *J Neurochem*. 2008; 105(5):1820–33. Epub 2008/02/06. <https://doi.org/10.1111/j.1471-4159.2008.05279.x> PMID: 18248608; PubMed Central PMCID: PMC2673995.
35. Kobayashi T, Yamanaka T, Jacobs JM, Teixeira F, Suzuki K. The Twitcher mouse: an enzymatically authentic model of human globoid cell leukodystrophy (Krabbe disease). *Brain Res*. 1980; 202(2):479–83. Epub 1980/12/08. [https://doi.org/10.1016/0006-8993\(80\)90159-6](https://doi.org/10.1016/0006-8993(80)90159-6) PMID: 7437911.
36. Kondo Y, Wenger DA, Gallo V, Duncan ID. Galactocerebrosidase-deficient oligodendrocytes maintain stable central myelin by exogenous replacement of the missing enzyme in mice. *Proc Natl Acad Sci U S A*. 2005; 102(51):18670–5. Epub 2005/12/15. <https://doi.org/10.1073/pnas.0506473102> PMID: 16352725; PubMed Central PMCID: PMC1317926.
37. Mohri I, Taniike M, Taniguchi H, Kanekiyo T, Aritake K, Inui T, et al. Prostaglandin D2-mediated microglia/astrocyte interaction enhances astrogliosis and demyelination in twitcher. *J Neurosci*. 2006; 26(16):4383–93. Epub 2006/04/21. <https://doi.org/10.1523/JNEUROSCI.4531-05.2006> PMID: 16624958; PubMed Central PMCID: PMC6673986.
38. Lanciotti A, Brignone MS, Macioce P, Visentin S, Ambrosini E. Human iPSC-Derived Astrocytes: A Powerful Tool to Study Primary Astrocyte Dysfunction in the Pathogenesis of Rare Leukodystrophies. *Int J Mol Sci*. 2021; 23(1). Epub 2022/01/12. <https://doi.org/10.3390/ijms23010274> PMID: 35008700; PubMed Central PMCID: PMC8745131.
39. Messing A. Alexander disease. *Handb Clin Neurol*. 2018; 148:693–700. Epub 2018/02/27. <https://doi.org/10.1016/B978-0-444-64076-5.00044-2> PMID: 29478608.
40. Dietrich J, Lacagnina M, Gass D, Richfield E, Mayer-Proschel M, Noble M, et al. EIF2B5 mutations compromise GFAP+ astrocyte generation in vanishing white matter leukodystrophy. *Nat Med*. 2005; 11(3):277–83. Epub 2005/02/22. <https://doi.org/10.1038/nm1195> PMID: 15723074.
41. Bugiani M, Boor I, van Kollenburg B, Postma N, Polder E, van Berkel C, et al. Defective glial maturation in vanishing white matter disease. *J Neuropathol Exp Neurol*. 2011; 70(1):69–82. Epub 2010/12/16. <https://doi.org/10.1097/NEN.0b013e318203ae74> PMID: 21157376; PubMed Central PMCID: PMC4135437.
42. Bugiani M, Vuong C, Breur M, van der Knaap MS. Vanishing white matter: a leukodystrophy due to astrocytic dysfunction. *Brain Pathol*. 2018; 28(3):408–21. Epub 2018/05/10. <https://doi.org/10.1111/bpa.12606> PMID: 29740943.
43. Gortz AL, Peferoen LAN, Gerritsen WH, van Noort JM, Bugiani M, Amor S. Heat shock protein expression in cerebral X-linked adrenoleukodystrophy reveals astrocyte stress prior to myelin loss. *Neuropathol Appl Neurobiol*. 2018; 44(4):363–76. Epub 2017/03/21. <https://doi.org/10.1111/nan.12399> PMID: 28319253.
44. Lanciotti A, Brignone MS, Bertini E, Petrucci TC, Aloisi F, Ambrosini E. Astrocytes: Emerging Stars in Leukodystrophy Pathogenesis. *Transl Neurosci*. 2013; 4(2). Epub 2013/12/18. <https://doi.org/10.2478/s13380-013-0118-1> PMID: 24340223; PubMed Central PMCID: PMC3856885.
45. Verkhatsky A, Sofroniew MV, Messing A, deLanerolle NC, Rempé D, Rodriguez JJ, et al. Neurological diseases as primary gliopathies: a reassessment of neurocentrism. *ASN Neuro*. 2012; 4(3). Epub 2012/02/22. <https://doi.org/10.1042/AN20120010> PMID: 22339481; PubMed Central PMCID: PMC3320215.
46. Takahashi K, Tanabe K, Ohnuki M, Narita M, Ichisaka T, Tomoda K, et al. Induction of pluripotent stem cells from adult human fibroblasts by defined factors. *Cell*. 2007; 131(5):861–72. Epub 2007/11/24. <https://doi.org/10.1016/j.cell.2007.11.019> PMID: 18035408.
47. Meng XL, Shen JS, Kawagoe S, Ohashi T, Brady RO, Eto Y. Induced pluripotent stem cells derived from mouse models of lysosomal storage disorders. *Proc Natl Acad Sci U S A*. 2010; 107(17):7886–91. Epub 2010/04/14. <https://doi.org/10.1073/pnas.1002758107> PMID: 20385825; PubMed Central PMCID: PMC2867869.
48. Mangiameli E, Cecchele A, Morena F, Sanvito F, Matafora V, Cattaneo A, et al. Human iPSC-based neurodevelopmental models of globoid cell leukodystrophy uncover patient- and cell type-specific disease phenotypes. *Stem Cell Reports*. 2021; 16(6):1478–95. Epub 2021/05/15. <https://doi.org/10.1016/j.stemcr.2021.04.011> PMID: 33989519; PubMed Central PMCID: PMC8190599.
49. Rafi MA, Luzi P, Chen YQ, Wenger DA. A large deletion together with a point mutation in the GALC gene is a common mutant allele in patients with infantile Krabbe disease. *Hum Mol Genet*. 1995; 4(8):1285–9. Epub 1995/08/01. <https://doi.org/10.1093/hmg/4.8.1285> PMID: 7581365.
50. Liu GH, Qu J, Suzuki K, Nivet E, Li M, Montserrat N, et al. Progressive degeneration of human neural stem cells caused by pathogenic LRRK2. *Nature*. 2012; 491(7425):603–7. <https://doi.org/10.1038/nature11557> PMID: 23075850; PubMed Central PMCID: PMC3504651.
51. Li W, Sun W, Zhang Y, Wei W, Ambasadhan R, Xia P, et al. Rapid induction and long-term self-renewal of primitive neural precursors from human embryonic stem cells by small molecule inhibitors.

- Proc Natl Acad Sci U S A. 2011; 108(20):8299–304. Epub 2011/04/29. <https://doi.org/10.1073/pnas.1014041108> PMID: 21525408; PubMed Central PMCID: PMC3100988.
52. Roybon L, Lamas NJ, Garcia AD, Yang EJ, Sattler R, Lewis VJ, et al. Human stem cell-derived spinal cord astrocytes with defined mature or reactive phenotypes. *Cell Rep*. 2013; 4(5):1035–48. Epub 2013/09/03. <https://doi.org/10.1016/j.celrep.2013.06.021> PMID: 23994478; PubMed Central PMCID: PMC4229657.
 53. Chandrasekaran A, Avci HX, Leist M, Kobolak J, Dinnyes A. Astrocyte Differentiation of Human Pluripotent Stem Cells: New Tools for Neurological Disorder Research. *Frontiers in cellular neuroscience*. 2016; 10:215. <https://doi.org/10.3389/fncel.2016.00215> PMID: 27725795; PubMed Central PMCID: PMC5035736.
 54. Haenseler W, Sansom SN, Buchrieser J, Newey SE, Moore CS, Nicholls FJ, et al. A Highly Efficient Human Pluripotent Stem Cell Microglia Model Displays a Neuronal-Co-culture-Specific Expression Profile and Inflammatory Response. *Stem Cell Reports*. 2017; 8(6):1727–42. Epub 2017/06/08. <https://doi.org/10.1016/j.stemcr.2017.05.017> PMID: 28591653; PubMed Central PMCID: PMC5470330.
 55. van Wilgenburg B, Browne C, Vowles J, Cowley SA. Efficient, long term production of monocyte-derived macrophages from human pluripotent stem cells under partly-defined and fully-defined conditions. *PLoS One*. 2013; 8(8):e71098. Epub 2013/08/21. <https://doi.org/10.1371/journal.pone.0071098> PMID: 23951090; PubMed Central PMCID: PMC3741356.
 56. Brownjohn PW, Smith J, Solanki R, Lohmann E, Houlden H, Hardy J, et al. Functional Studies of Missense TREM2 Mutations in Human Stem Cell-Derived Microglia. *Stem Cell Reports*. 2018; 10(4):1294–307. Epub 2018/04/03. <https://doi.org/10.1016/j.stemcr.2018.03.003> PMID: 29606617; PubMed Central PMCID: PMC5998752.
 57. Vitner EB, Salomon R, Farfel-Becker T, Meshcheriakova A, Ali M, Klein AD, et al. RIPK3 as a potential therapeutic target for Gaucher's disease. *Nat Med*. 2014; 20(2):204–8. Epub 2014/01/21. <https://doi.org/10.1038/nm.3449> PMID: 24441827.
 58. Cesani M, Cavalca E, Macco R, Leoncini G, Terreni MR, Lioroli L, et al. Metallothioneins as dynamic markers for brain disease in lysosomal disorders. *Ann Neurol*. 2014; 75(1):127–37. Epub 2013/11/19. <https://doi.org/10.1002/ana.24053> PMID: 24242821; PubMed Central PMCID: PMC4237725.
 59. LeVine SM, Brown DC. IL-6 and TNFalpha expression in brains of twitcher, quaking and normal mice. *J Neuroimmunol*. 1997; 73(1–2):47–56. Epub 1997/03/01. [https://doi.org/10.1016/s0165-5728\(96\)00166-x](https://doi.org/10.1016/s0165-5728(96)00166-x) PMID: 9058758.
 60. Hanada K. Serine palmitoyltransferase, a key enzyme of sphingolipid metabolism. *Biochim Biophys Acta*. 2003; 1632(1–3):16–30. Epub 2003/06/05. [https://doi.org/10.1016/s1388-1981\(03\)00059-3](https://doi.org/10.1016/s1388-1981(03)00059-3) PMID: 12782147.
 61. Tcw J, Wang M, Pimenova AA, Bowles KR, Hartley BJ, Lacin E, et al. An Efficient Platform for Astrocyte Differentiation from Human Induced Pluripotent Stem Cells. *Stem Cell Reports*. 2017; 9(2):600–14. Epub 2017/08/02. <https://doi.org/10.1016/j.stemcr.2017.06.018> PMID: 28757165; PubMed Central PMCID: PMC5550034.
 62. Corado CR, Pinkstaff J, Jiang X, Galban EM, Fisher SJ, Scholler O, et al. Cerebrospinal fluid and serum glycosphingolipid biomarkers in canine globoid cell leukodystrophy (Krabbe Disease). *Mol Cell Neurosci*. 2020; 102:103451. Epub 2019/12/04. <https://doi.org/10.1016/j.mcn.2019.103451> PMID: 31794880; PubMed Central PMCID: PMC7032565.
 63. Esch SW, Williams TD, Biswas S, Chakrabarty A, LeVine SM. Sphingolipid profile in the CNS of the twitcher (globoid cell leukodystrophy) mouse: a lipidomics approach. *Cell Mol Biol (Noisy-le-grand)*. 2003; 49(5):779–87. Epub 2003/10/08. PMID: 14528915.
 64. Katsel P, Li C, Haroutunian V. Gene expression alterations in the sphingolipid metabolism pathways during progression of dementia and Alzheimer's disease: a shift toward ceramide accumulation at the earliest recognizable stages of Alzheimer's disease? *Neurochem Res*. 2007; 32(4–5):845–56. Epub 2007/03/08. <https://doi.org/10.1007/s11064-007-9297-x> PMID: 17342407.
 65. Cutler RG, Kelly J, Storie K, Pedersen WA, Tammara A, Hatanpaa K, et al. Involvement of oxidative stress-induced abnormalities in ceramide and cholesterol metabolism in brain aging and Alzheimer's disease. *Proc Natl Acad Sci U S A*. 2004; 101(7):2070–5. Epub 2004/02/19. <https://doi.org/10.1073/pnas.0305799101> PMID: 14970312; PubMed Central PMCID: PMC357053.
 66. Mielke MM, Maetzler W, Haughey NJ, Bandaru VV, Savica R, Deuschle C, et al. Plasma ceramide and glucosylceramide metabolism is altered in sporadic Parkinson's disease and associated with cognitive impairment: a pilot study. *PLoS One*. 2013; 8(9):e73094. Epub 2013/09/24. <https://doi.org/10.1371/journal.pone.0073094> PMID: 24058461; PubMed Central PMCID: PMC3776817.
 67. Xing Y, Tang Y, Zhao L, Wang Q, Qin W, Ji X, et al. Associations between plasma ceramides and cognitive and neuropsychiatric manifestations in Parkinson's disease dementia. *J Neurol Sci*. 2016; 370:82–7. Epub 2016/10/25. <https://doi.org/10.1016/j.jns.2016.09.028> PMID: 27772793.

68. Cutler RG, Pedersen WA, Camandola S, Rothstein JD, Mattson MP. Evidence that accumulation of ceramides and cholesterol esters mediates oxidative stress-induced death of motor neurons in amyotrophic lateral sclerosis. *Ann Neurol*. 2002; 52(4):448–57. Epub 2002/09/27. <https://doi.org/10.1002/ana.10312> PMID: 12325074.
69. Dodge JC, Treleaven CM, Pacheco J, Cooper S, Bao C, Abraham M, et al. Glycosphingolipids are modulators of disease pathogenesis in amyotrophic lateral sclerosis. *Proc Natl Acad Sci U S A*. 2015; 112(26):8100–5. Epub 2015/06/10. <https://doi.org/10.1073/pnas.1508767112> PMID: 26056266; PubMed Central PMCID: PMC4491749.
70. Wang G, Bieberich E. Sphingolipids in neurodegeneration (with focus on ceramide and S1P). *Adv Biol Regul*. 2018; 70:51–64. Epub 2018/10/06. <https://doi.org/10.1016/j.jbior.2018.09.013> PMID: 30287225; PubMed Central PMCID: PMC6251739.
71. Kolesnick RN, Kronke M. Regulation of ceramide production and apoptosis. *Annu Rev Physiol*. 1998; 60:643–65. Epub 1998/04/29. <https://doi.org/10.1146/annurev.physiol.60.1.643> PMID: 9558480.
72. Ballou LR, Laulederkind SJ, Rosloniec EF, Raghov R. Ceramide signalling and the immune response. *Biochim Biophys Acta*. 1996; 1301(3):273–87. Epub 1996/06/11. [https://doi.org/10.1016/0005-2760\(96\)00004-5](https://doi.org/10.1016/0005-2760(96)00004-5) PMID: 8664339.
73. Lee JT, Xu J, Lee JM, Ku G, Han X, Yang DI, et al. Amyloid-beta peptide induces oligodendrocyte death by activating the neutral sphingomyelinase-ceramide pathway. *J Cell Biol*. 2004; 164(1):123–31. Epub 2004/01/08. <https://doi.org/10.1083/jcb.200307017> PMID: 14709545; PubMed Central PMCID: PMC2171973.
74. El Alwani M, Wu BX, Obeid LM, Hannun YA. Bioactive sphingolipids in the modulation of the inflammatory response. *Pharmacol Ther*. 2006; 112(1):171–83. Epub 2006/06/09. <https://doi.org/10.1016/j.pharmthera.2006.04.004> PMID: 16759708.
75. Maceyka M, Spiegel S. Sphingolipid metabolites in inflammatory disease. *Nature*. 2014; 510(7503):58–67. Epub 2014/06/06. <https://doi.org/10.1038/nature13475> PMID: 24899305; PubMed Central PMCID: PMC4320971.
76. Sato H, Tomimoto H, Ohtani R, Kitano T, Kondo T, Watanabe M, et al. Astroglial expression of ceramide in Alzheimer's disease brains: a role during neuronal apoptosis. *Neuroscience*. 2005; 130(3):657–66. Epub 2004/12/14. <https://doi.org/10.1016/j.neuroscience.2004.08.056> PMID: 15590150.
77. de Wit NM, den Hoedt S, Martinez-Martinez P, Rozemuller AJ, Mulder MT, de Vries HE. Astrocytic ceramide as possible indicator of neuroinflammation. *J Neuroinflammation*. 2019; 16(1):48. Epub 2019/02/26. <https://doi.org/10.1186/s12974-019-1436-1> PMID: 30803453; PubMed Central PMCID: PMC6388480.
78. Wang G, Dinkins M, He Q, Zhu G, Poirier C, Campbell A, et al. Astrocytes secrete exosomes enriched with proapoptotic ceramide and prostate apoptosis response 4 (PAR-4): potential mechanism of apoptosis induction in Alzheimer disease (AD). *J Biol Chem*. 2012; 287(25):21384–95. Epub 2012/04/26. <https://doi.org/10.1074/jbc.M112.340513> PMID: 22532571; PubMed Central PMCID: PMC3375560.
79. Gowrishankar S, Cologna SM, Givogri MI, Bongarzone ER. Deregulation of signalling in genetic conditions affecting the lysosomal metabolism of cholesterol and galactosyl-sphingolipids. *Neurobiol Dis*. 2020; 146:105142. Epub 2020/10/21. <https://doi.org/10.1016/j.nbd.2020.105142> PMID: 33080336.
80. Grosch S, Schiffmann S, Geisslinger G. Chain length-specific properties of ceramides. *Prog Lipid Res*. 2012; 51(1):50–62. Epub 2011/12/03. <https://doi.org/10.1016/j.plipres.2011.11.001> PMID: 22133871.
81. Sassa T, Suto S, Okayasu Y, Kihara A. A shift in sphingolipid composition from C24 to C16 increases susceptibility to apoptosis in HeLa cells. *Biochim Biophys Acta*. 2012; 1821(7):1031–7. Epub 2012/05/15. <https://doi.org/10.1016/j.bbali.2012.04.008> PMID: 22579584.
82. Rama Rao KV, Kielian T. Astrocytes and lysosomal storage diseases. *Neuroscience*. 2016; 323:195–206. Epub 2015/06/04. <https://doi.org/10.1016/j.neuroscience.2015.05.061> PMID: 26037807; PubMed Central PMCID: PMC4664580.
83. Di Malta C, Fryer JD, Settembre C, Ballabio A. Astrocyte dysfunction triggers neurodegeneration in a lysosomal storage disorder. *Proc Natl Acad Sci U S A*. 2012; 109(35):E2334–42. Epub 2012/07/25. <https://doi.org/10.1073/pnas.1209577109> PMID: 22826245; PubMed Central PMCID: PMC3435187.
84. Takata K, Kozaki T, Lee CZW, Thion MS, Otsuka M, Lim S, et al. Induced-Pluripotent-Stem-Cell-Derived Primitiv Macrophages Provide a Platform for Modeling Tissue-Resident Macrophage Differentiation and Function. *Immunity*. 2017; 47(1):183–98 e6. Epub 2017/07/21. <https://doi.org/10.1016/j.immuni.2017.06.017> PMID: 28723550.
85. Nicaise AM, Bongarzone ER, Crocker SJ. A microglial hypothesis of globoid cell leukodystrophy pathology. *J Neurosci Res*. 2016; 94(11):1049–61. Epub 2016/09/18. <https://doi.org/10.1002/jnr.23773> PMID: 27638591; PubMed Central PMCID: PMC5027969.
86. Potter GB, Petryniak MA. Neuroimmune mechanisms in Krabbe's disease. *J Neurosci Res*. 2016; 94(11):1341–8. Epub 2016/09/18. <https://doi.org/10.1002/jnr.23804> PMID: 27638616; PubMed Central PMCID: PMC5129482.

87. Scott-Hewitt NJ, Folts CJ, Hogestyn JM, Piester G, Mayer-Proschel M, Noble MD. Heterozygote galactocerebrosidase (GALC) mutants have reduced remyelination and impaired myelin debris clearance following demyelinating injury. *Hum Mol Genet.* 2017; 26(15):2825–37. Epub 2017/06/03. <https://doi.org/10.1093/hmg/ddx153> PMID: 28575206; PubMed Central PMCID: PMC5886101.
88. Borda JT, Alvarez X, Mohan M, Ratterree MS, Phillippi-Falkenstein K, Lackner AA, et al. Clinical and immunopathologic alterations in rhesus macaques affected with globoid cell leukodystrophy. *Am J Pathol.* 2008; 172(1):98–111. Epub 2008/01/01. <https://doi.org/10.2353/ajpath.2008.070404> PMID: 18165263; PubMed Central PMCID: PMC2189619.
89. Ouali Alami N, Schurr C, Olde Heuvel F, Tang L, Li Q, Tasdogan A, et al. NF-kappaB activation in astrocytes drives a stage-specific beneficial neuroimmunological response in ALS. *EMBO J.* 2018; 37(16). Epub 2018/06/08. <https://doi.org/10.15252/embj.201798697> PMID: 29875132; PubMed Central PMCID: PMC6092622.
90. Kondo Y, Adams JM, Vanier MT, Duncan ID. Macrophages counteract demyelination in a mouse model of globoid cell leukodystrophy. *J Neurosci.* 2011; 31(10):3610–24. Epub 2011/03/11. <https://doi.org/10.1523/JNEUROSCI.6344-10.2011> PMID: 21389217; PubMed Central PMCID: PMC3086602.
91. Li Y, Xu Y, Benitez BA, Nagree MS, Dearborn JT, Jiang X, et al. Genetic ablation of acid ceramidase in Krabbe disease confirms the psychosine hypothesis and identifies a new therapeutic target. *Proc Natl Acad Sci U S A.* 2019; 116(40):20097–103. Epub 2019/09/19. <https://doi.org/10.1073/pnas.1912108116> PMID: 31527255; PubMed Central PMCID: PMC6778236.
92. Zaccariotto E, Cachon-Gonzalez MB, Wang B, Lim S, Hirth B, Park H, et al. A novel brain-penetrant oral UGT8 inhibitor decreases in vivo galactosphingolipid biosynthesis in murine Krabbe disease. *Biomed Pharmacother.* 2022; 149:112808. Epub 2022/03/16. <https://doi.org/10.1016/j.biopha.2022.112808> PMID: 35290889.
93. Babcock MC, Mikulka CR, Wang B, Chandriani S, Chandra S, Xu Y, et al. Substrate reduction therapy for Krabbe disease and metachromatic leukodystrophy using a novel ceramide galactosyltransferase inhibitor. *Sci Rep.* 2021; 11(1):14486. Epub 2021/07/16. <https://doi.org/10.1038/s41598-021-93601-1> PMID: 34262084; PubMed Central PMCID: PMC8280112.
94. Biswas S, Biesiada H, Williams TD, LeVine SM. Substrate reduction intervention by L-cycloserine in twitcher mice (globoid cell leukodystrophy) on a B6;CAST/Ei background. *Neurosci Lett.* 2003; 347(1):33–6. Epub 2003/07/17. [https://doi.org/10.1016/s0304-3940\(03\)00633-5](https://doi.org/10.1016/s0304-3940(03)00633-5) PMID: 12865135.
95. LeVine SM, Pedchenko TV, Bronshteyn IG, Pinson DM. L-cycloserine slows the clinical and pathological course in mice with globoid cell leukodystrophy (twitcher mice). *J Neurosci Res.* 2000; 60(2):231–6. Epub 2000/03/31. [https://doi.org/10.1002/\(SICI\)1097-4547\(20000415\)60:2<231::AID-JNR12>3.0.CO;2-E](https://doi.org/10.1002/(SICI)1097-4547(20000415)60:2<231::AID-JNR12>3.0.CO;2-E) PMID: 10740228.
96. Maceyka M, Harikumar KB, Milstien S, Spiegel S. Sphingosine-1-phosphate signaling and its role in disease. *Trends Cell Biol.* 2012; 22(1):50–60. Epub 2011/10/18. <https://doi.org/10.1016/j.tcb.2011.09.003> PMID: 22001186; PubMed Central PMCID: PMC3253987.
97. Fyrst H, Saba JD. An update on sphingosine-1-phosphate and other sphingolipid mediators. *Nat Chem Biol.* 2010; 6(7):489–97. Epub 2010/06/19. <https://doi.org/10.1038/nchembio.392> PMID: 20559316; PubMed Central PMCID: PMC3001344.
98. Bechet S, O'Sullivan SA, Yssel J, Fagan SG, Dev KK. Fingolimod Rescues Demyelination in a Mouse Model of Krabbe's Disease. *J Neurosci.* 2020; 40(15):3104–18. Epub 2020/03/05. <https://doi.org/10.1523/JNEUROSCI.2346-19.2020> PMID: 32127495; PubMed Central PMCID: PMC7141882.
99. Ungari S, Montepeloso A, Morena F, Cocchiarella F, Recchia A, Martino S, et al. Design of a regulated lentiviral vector for hematopoietic stem cell gene therapy of globoid cell leukodystrophy. *Mol Ther Methods Clin Dev.* 2015; 2:15038. Epub 2015/10/29. <https://doi.org/10.1038/mtm.2015.38> PMID: 26509184; PubMed Central PMCID: PMC4605225.
100. Hu P, Li Y, Nikolaishvili-Feinberg N, Scesa G, Bi Y, Pan D, et al. Hematopoietic Stem cell transplantation and lentiviral vector-based gene therapy for Krabbe's disease: Present convictions and future prospects. *J Neurosci Res.* 2016; 94(11):1152–68. Epub 2016/09/18. <https://doi.org/10.1002/jnr.23847> PMID: 27638600; PubMed Central PMCID: PMC5027985.